Gross morphology, radiology and computed tomography of the ear of the southern white rhinoceros (*Ceratotherium simum simum*)

By

Dr Mickaël Patrice Robert

Submitted in fulfilment of the degree

Master of Science
Veterinary Science

Department of Companion Animal Clinical Studies
Faculty of Veterinary Science
University of Pretoria

January 2020

Supervisor: Prof Gerhard Steenkamp
Co-supervisor: Prof Ann Carstens

DECLARATION OF ORIGINALITY

UNIVERSITY OF PRETORIA

FACULTY OF VETERINARY SCIENCE

DECLARATION OF ORIGINALITY

This document must be signed and submitted with every essay, report, project, assignment, mini-dissertation, dissertation and/or thesis

Full names of student: Mickaël Patrice Robert

Student number: 04944764

Declaration:

1. I understand what plagiarism is and am aware of the University's policy in this regard.

2. I declare that this dissertation, "Gross morphology, radiology and computed tomography of the ear of the southern white rhinoceros (*Ceratotherium simum simum*)" is my own original work. Where other people's work has been used (either from a printed source, Internet or any other source), this has been properly acknowledged and referenced in accordance with departmental requirements.

3. I have not used work previously produced by another student or any other person to hand in as my own.

4. I have not allowed, and will not allow, anyone to copy my work with the intention of passing it off as his or her own work.

22 January 2020

Signature of student:

Signature of supervisor: ………………………………………

ACKNOWLEDGEMENTS

To Prof. Gerhard Steenkamp, my promoter, for taking me with you to treat a rhino when I just arrived in the country, for offering me this topic and guiding me along this project.

To Prof. Ann Cartens, for accepting being my co-promoter, for your permanent kindness and assistance with image interpretation.

To Prof. Emma Hooijberg, for always being positive during my guidance committee meetings.

To my colleagues at the Equine Clinic, who supported me during this project.

To Dr. Michelle Otto, from Buffalo Dream Ranch, who provided us with 2 baby rhino heads when we were struggling to get samples.

To Anelia Vorster and the Imaging team of the Netcare Montana Hospital for providing us with amazing CT and MRI images, always with a smile and a cup of coffee.

To Abram Komane for keeping my samples safe in the wet skills laboratory at Onderstepoort.

To the RADTOM team of NECSA, especially Dr. Frikkie de Beer, for the stunning micro-CT images and your understanding despite the delays in our project.

To my parents, who always encouraged me to be a vet and to follow my dreams.

To my love Fleur, who followed me in this crazy South African adventure and supports me every day.

SUMMARY

Gross morphology, radiology and computed tomography of the ear of the southern white rhinoceros (*Ceratotherium simum simum*)

By: Mickaël Robert

Supervisor: Prof Gerhard Steenkamp

Co-supervisor: Prof Ann Carstens

Department: Companion Animal Clinical Studies

Degree: MSc

Since 2008 there has been a dramatic increase in poaching of rhinoceroses in Africa. Today, the southern white rhinoceros is classified as Near Threatened with less than 20000 individuals left. The ear of the rhinoceros appears to be an important organ in the animal's behaviour and thermoregulation, in population management and also for clinical use. Despite its important roles, there is currently only fragmented information available concerning the rhinoceros's gross ear anatomy as well as radiographic and computed tomographic (CT) anatomy. The aim of this study is to fill this void describing the gross, radiographic and CT anatomy of the ear of the southern white rhinoceros following the standard international veterinary anatomical nomenclature.

We used seven intact ears belonging to four southern white rhinoceroses (3 cadavers plus 1 clinical case) of different age (from neonate to adult) to perform radiographic, CT and micro-CT studies before dissecting four of them. We described the gross anatomy of the cartilages, muscles, particular vessels of the ear and associated organs, we presented radiographic views and CT protocols that can be used to assess this region as well as the imaged structures, and we reported on the micro-anatomy of the southern white rhinoceros ear using micro-CT, allowing tridimensional virtual models of the middle and inner ears to be displayed.

The findings of this study will be useful to anatomists, radiologists and wildlife veterinarians, and will also hopefully pave the way for further research providing even more detail of this fascinating but difficult to investigate region.

KEY WORDS

White rhinoceros, ear, morphology, radiography, computed tomography, micro-CT

TABLE OF CONTENT

LIST OF FIGURES

LIST OF TABLES

LIST OF ABBREVIATIONS

CITES	Convention on International Trade in Endangered Species of Wild Fauna and Flora
CR	Computed radiography
CT	Computed tomography
DICOM	Digital imaging and communications in medicine
DR	Digital radiography
DV	Dorso-ventral
HU	Hounsfield units
ICVGAN	International Committee on Veterinary Gross Anatomical Nomenclature
IUCN	Union for Conservation of Nature and Natural Resources
Jpeg	Joint Photographic Experts Group
kV	Kilovolt
LL	Latero-lateral
mAs	Milliampere-second
micro-CT	Micro-computed tomography
MIXRAD	Micro-Focus X-ray Tomography Facility
MRI	Magnetic resonance imaging
NECSA	South African Nuclear Energy Corporation
OVAH	Onderstepoort Veterinary Academic Hospital
Rhino	Rhinoceros
Rhinos	Rhinoceroses
Tiff	Tagged Image File Format
TMJ	Temporo-mandibular joint
WL	Window level
WW	Window width

CHAPTER 1: INTRODUCTION

1.1 Background

Since 2008 there has been a dramatic increase in poaching of rhinoceroses in Africa. The ear of the rhinoceros appears to be an important organ in the animal's behavior and thermoregulation, in population management and also for clinical use.

1.2 Problem Statement

Despite its important roles, there is currently only fragmented information available for anatomists, radiologists and wildlife veterinarians about the rhinoceros's ear compared to what is published in domestic animals and people.

1.3 Objectives

The aim of this study is to describe the gross, radiographic, CT and micro-CT anatomy of the ear of the southern white rhinoceros following the standard international veterinary anatomical nomenclature (ICVGAN 2017).

Particularly, we anticipate to:

- Describe the normal gross anatomy of the southern white rhinoceros ear
- Show that the ear of the white rhinoceros shares common traits with that of other domestic mammals
- Describe the radiographic views that can be used to evaluate the ear region of the southern white rhinoceros
- Describe the radiographic anatomy of the southern white rhinoceros ear
- Describe the CT and micro-CT anatomy of the southern white rhinoceros ear using human and equine references

1.4 Benefits of this study

The findings of this study will be useful to:

- anatomists and zoologists, providing them with gross and micro-anatomical details that have not been reported previously about the ear of the southern white rhinoceros
- radiologists, giving them indications on what can be expected from radiographs and CT when investigating this organ, and also suggesting some imaging views and protocols
- wildlife veterinarians dealing with southern white rhinoceros' ears, bringing them clinically relevant anatomical details and radiographic tips to increase their chances of obtaining diagnostic images

This study will also hopefully pave the way for further research providing even more detail of this fascinating but challenging to investigate area.

CHAPTER 2: LITERATURE REVIEW

2.1 Introduction

Since 2008 there has been a dramatic increase in poaching of rhinoceroses in Africa (Anonymous 2018b). Today, the southern white rhinoceros is classified as Near Threatened (Emslie 2012). The most recent estimates for this species are only 20000 animals remaining in Africa (Knight 2017). In the rhinoceros, the pinna of the ear appears to be an important organ in the animal's behaviour and thermoregulation, in population management and also for clinical use (Dinerstein 2011; Miller & Buss 2014; Ngene et al. 2011; Owen-Smith 2013). It can display clinical signs of systemic disease and can also be used to collect blood samples, administer drugs or monitor anaesthesia. Despite these important roles, only a few studies were found describing the white rhinoceros ear anatomy compared to several descriptions in domestic animals (Barone 2010a; Barone 2010b; Barone 2010c; Barone 2011; Collin 2006). Additionally, very little diagnostic imaging data have been published on the ear region of the rhinoceros, regardless of species and subspecies (Fritsch et al. 2004; Schellhorn 2018).

2.2 The southern white rhinoceros (*Ceratotherium simum simum*)

Rhinoceroses belong to the Class *Mammalia*, Order *Perissodactyla*, Family *Rhinocerotidae* (Dinerstein 2011).

The white rhinoceros, also called square-lipped rhinoceros or grass rhinoceros, is the largest of the five extant rhinoceros species and one of the two African species (Owen-Smith 2013). It belongs to the subfamily *Dicerotinae*. Whereas two subspecies are officially recognized, the southern white rhinoceros *Ceratotherium simum simum* in southern Africa, and the northern white rhinoceros *Ceratotherium simum cottoni*, the latter is considered nearly extinct after the last male died in March 2018, leaving only two females in Kenya (Anonymous 2018b; Lemonde.fr 2018).

According to the International Union for Conservation of Nature and Natural Resources (IUCN), the southern white rhinoceros is classified as Near Threatened due to the continued and increased poaching threat and increasing illegal demand for horn. Whereas rhino horn has traditionally been used for daggers in Yemen and in Chinese traditional medicine to treat fever, today Vietnam is thought to be the largest consumer of rhino horn. In this country, rhino horn is used as a health tonic, is believed to cure cancer, but it is apparently also a status symbol, a means for people to flaunt their wealth. Its value on the black market could reach 100000 US $/kg (Anonymous 2012; Anonymous 2018a; Emslie 2012; Emslie et al. 2016; Milliken et al. 2012; Robin des Bois 2018). In recent years poaching levels have dramatically increased in major range states such as Namibia, Zimbabwe, Kenya and South Africa (Milliken et al. 2009). Since 2013, more than 1000 rhinoceros are poached annually in South Africa (Knight 2017; Robin des Bois 2018; TRAFFIC 2018).

Even though the southern white rhinoceros was on the brink of extinction by the end of the 19th century, its recovery from just one small population of approximately 20 to 200 animals in KwaZulu-Natal has been recognized as among the world's greatest conservation success stories. South Africa currently remains the stronghold for this subspecies with an estimated population of 18000 animals occurring in numerous state protected areas and private reserves (Emslie 2012; Owen-Smith 2013).

All the African rhinoceros species were listed on the Convention on International Trade in Endangered Species of Wild Fauna and Flora (CITES) Appendix I in 1977, prohibiting any commercial trade. However, the South African population of southern white rhinoceros was down listed in 1994 to Appendix II, as was the Swaziland population in 2004, but only for trade in live animals to "approved and acceptable destinations" and for the export of hunting trophies (CITES 2017).

2.3 The ear of domestic mammals

The ear (*auris*) or vestibulo-cochlear organ (*organum vestibulocochleare*) is a sensory organ located in the temporal bone and intended for the perception of sounds but also changes of position of the body and more particularly of the head. It consists of an external -, middle - and inner ear (Collin 2006).

1. The external ear (*auris externa*) is designed to pick up sounds and allow entrance through the auricle or pinna into the ear canal to the tympanic membrane or eardrum. In the domestic mammals, it is very different in appearance, size and orientation depending on species, breed and even individuals (Barone 2010a). It is made up of three elastic cartilages: the auricular cartilage (*cartilago auriculae*), annular cartilage (*cartilago anularis*) and scutiform cartilage (*cartilago scutiformis*)(Figure 1). The skin covering the pinna is attached to the auricular cartilage by connective tissue. Extrinsic muscles ensure its mobility whereas intrinsic muscles maintain its shape (Barone 2010b).

The ear canal contains a cartilaginous part which is based on the tubular portion of both the auricular and annular cartilages, and an osseous part formed by the external acoustic meatus.

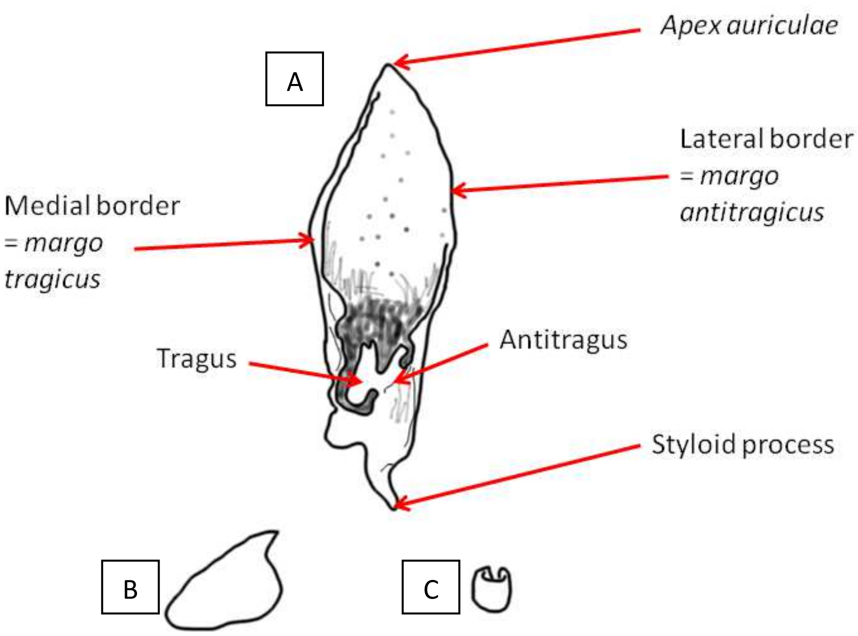

Figure 1: Cartilaginous components of the left external ear in the horse. A: Auricular cartilage; B: Scutiform cartilage; C: Annular cartilage. Modified from Collin (2006).

2. The middle ear (*auris media*) consists of the tympanic cavity, within the tuberous part of the temporal bone. It contains the ossicles of hearing and is made up of three parts: the atrium,

located medially to the tympanic membrane, the epitympanic recess above the latter, and a large ventral expansion, the tympanic bulla, the development of which varies greatly from one species to another (Barone 2010a). It is isolated from the external ear by the tympanic membrane and from the inner ear by a bony septum perforated by 2 small openings, the oval window (*fenestra vestibule*) and the round window (*fenestra cochleae*) separated by the promontory. The convex inner surface of the tympanic membrane adheres to the malleus shaft (Figure 2). The tympanic cord (*chorda tympani*) from the facial nerve runs against its upper part. The tympanic branch of the glossopharyngeal nerve passes on the ventral aspect of the promontory. The oval window is occupied by the base of the stapes and its annular ligament. The round window is closed by the secondary tympanic membrane which separates the middle ear from the tympanic ramp (*scala tympani*) of the cochlea.

The ossicles chain (*ossicula auditus*) together with the tympanic membrane form the organ of sound transmission. They provide the transmission of the eardrum vibrations to the structures of the inner ear, the base of the stapes transmitting vibrations to the perilymph, the liquid of the inner ear.

The auditory or Eustachian tube connects the middle ear to the pharynx. It consists of a bony component within the temporal bone and of a fibro-cartilaginous component. It allows renewal of air in the middle ear and the maintenance of an equal pressure either side of the tympanic membrane. It also allows evacuation of the tympanic mucosal secretions into the pharynx by means of its ciliated epithelium. In certain perissodactyls, such as equids and tapirs, and in some bats, a South American forest mouse, hyraxes and cetaceans, paired outpouchings of the Eustachian tubes called guttural pouches (*diverticulum tubae auditivae*) are found between the base of the cranium dorsally and the pharynx ventrally (Collin 2006; Freeman & Hardy 2012; Hinchcliffe & Pye 2009; Quse & Fernandes-Santos 2014). Possible functions of these pouches include being a resonating chamber for vocalization and a brain cooling system (Baptiste et al. 2000; Freeman & Hardy 2012).

3. The inner ear (*auris interna*) contains two sensory organs: firstly the cochlea - the organ of hearing, and secondly the utricle, saccule, and semicircular canals and their proprioceptive receptors which constitute the organ of equilibrium and record the changes of position of the body (Figure 2). The inner ear is located in the petrous part of the temporal bone, medial and caudal to the eardrum and is formed by the osseous labyrinth (*labyrinthus osseus*), in which the membranous labyrinth (*labyrinthus membranaceus*) is found. It contains two fluids: the endolymph in the membranous labyrinth and the perilymph around it, in the cavities of the osseous labyrinth. The perilymphatic space communicates with the subarachnoid space via the perilymphatic duct (Collin 2006).

The bony labyrinth is divided in three parts: the vestibule, semicircular canals and cochlea.

The vestibule is the middle part, continuing through the cochlea rostral. On its caudal side are the semicircular canals. On the internal wall of the oval window the vestibular ramp (*scala vestibule*) starts. Fibers of the vestibulo-cochlear nerve find their way through the *maculae cribrosae*. Three semicircular bony canals (*canales semicirculares*), anterior, posterior and lateral, perpendicular to each other, contain the membranous semicircular ducts (*ductus semicirculares*) caudal and dorsal to the vestibule. The cochlea is located cranial and ventral to the vestibule. It is a helicoidal canal around a central bone axis called modiolus containing the cochlear nerve centrally. The spiral canal starts at the vestibule and takes 3 turns in the horse before ending in a closed tip at the apex of the cochlea (Collin 2006).

The membranous labyrinth is a system of vesicles and ducts housed in the osseous labyrinth, suspended by connective tissue. The membranous vestibule contains two vesicles, the dorsal ovoid utricle (*utriculus*) and the ventral spherical saccule (*sacculus*). The former receives the membranous semicircular ducts whereas the latter covers the initial part of the membranous cochlear duct. They are united by the utriculosaccular duct (*ductus utriculosaccularis*). Maculae located in each of these vesicles, perpendicular to each other, record the linear accelerations and changes of position of the head. The membranous semicircular ducts communicate with the utricle, bathed in the perilymph, fixed by conjunctive trabeculae. A dilated portion, called the ampulla (*ampulla membranacea*), contains a sensory epithelium forming the ampullary crest (*crista ampullaris*) in each duct. They record circular accelerations and changes in position of the head and intervene in reflex oculogyric movements.

The cochlear duct starts through the vestibular cecum (*cecum vestibulare*) and ends with the cupular cecum (*cecum cupulare*). It communicates with the saccule by means of the *ductus reuniens*. The vestibular ramp opens in the vestibule; the tympanic ramp leads to the round window (Collin 2006).

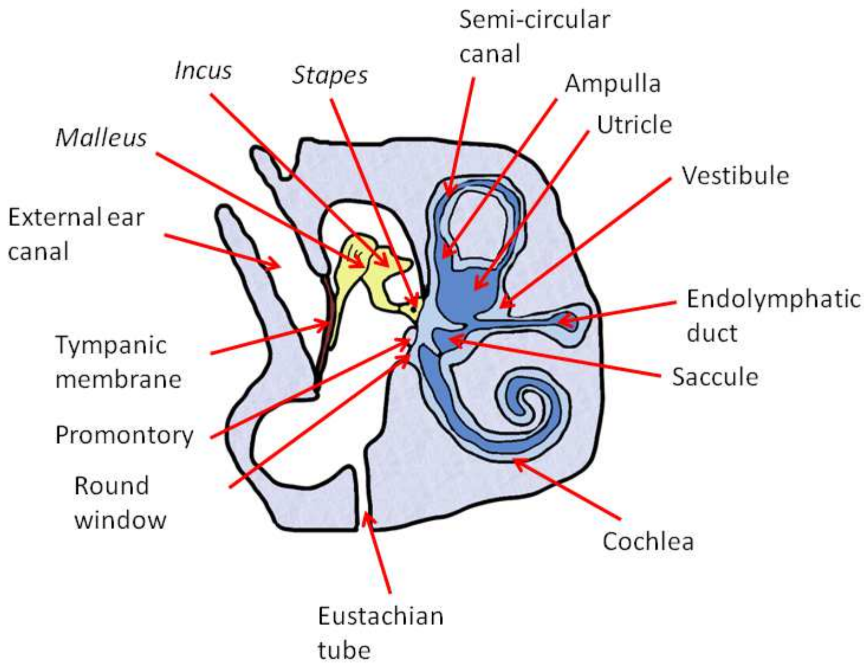

Figure 2: Illustration of the structures of the middle and inner ear in the horse. Modified from Collin (2006).

The different muscle layers, arterial and nerve supply of the ear, as well as the venous and lymphatic drainage, have been extensively described in the domestic mammals (Barone 2010c; Barone 2011).

2.4 The ear of the rhinoceros

2.4.1 Descriptive anatomy

Information relating to rhinoceros ear anatomy is rare. In the early 19th century, Vicq-D'Azyr and Cloquet presented a limited description of the rhinoceros ear (Vicq-D'Azyr & Cloquet 1819). They mentioned that in the Indian rhinoceros (*Rhinoceros unicornis*) pinna length was one foot and that the width between the "apophyses placed behind the holes of the ears" was 31cm. According to them, the "bone of the ear" was welded by the base around the auditory canal of the temporal bone; the internal auditory canal was small, oval, placed in the middle of the petrous temporal bone with an large rostro-caudal diameter; the auditory meatus has an almost vertical axis and the external auditory canal descends at an angle of 45°. They described large and straight pinnae mobile in every direction, with rare and stiff hairs on the edges compared to the smooth inner and outer surfaces. In the black rhinoceros (*Diceros bicornis*), the size of the ear was 8½ inches in length and 5 inches in width or 1 foot long with 6 inches apart. They noted a resemblance with the pig ear despite being smaller compared to the body size.

Owen (1866) mentioned that the petrous part of the temporal bone was very small, that the tympanic part was reduced to the frame of the membrane, and that it fused early on with the mastoid and squamous parts. He reported the auricle to be pedunculated, expanding into a moderate elliptical chamber from the upper part of the head. He also presented a detailed description of the rhinoceros's ossicles chain.

In 1873, Hyrtl (Hyrtl 1873) mentioned that the cochlear aqueduct (*ductus perilymphaticus*) is straight (not helicoidal) in the black rhinoceros. In 1970, Saban (Saban 1970) published an illustrated description of the musculature of the head and neck of the Indian rhinoceros after dissecting a specimen at the zoological garden of Vincennes.

The possible presence of guttural pouches in rhinoceroses has also been investigated. Indeed, numerous textbooks and recent articles mention that these paired outpouchings of the Eustachian tubes are present in the rhinoceros (Freeman & Hardy 2012; Hahn 2015; Lepage 2007; Pollock 2007; Rooney 1996). However recent dissections and computed tomographic (CT) studies showed that both the white - and Indian rhinoceros do not have guttural pouches (Endo et al. 1998; Endo et al. 2009). The author believes this earlier assumption came from a misinterpretation of a previous study describing the epipharyngeal bursa in rhinoceroses (Cave 1974). The latter is a median saccule having lympho-glandular functions, reportedly measuring 11cm long with a diameter of 4cm, overlying the entire length of the pharynx, between the base of the skull dorsally and the pharynx roof ventrally. Its counterpart is the pharyngeal recess (*recessus pharyngeus*) in Equidae. The French name "poches pharyngiennes" of this particular structure could indeed be misleading.

2.4.2 Diagnostic imaging data

Recently it was stated that bone pathology in rhinoceroses has long been overlooked since radiographic techniques, protocols, normal radiographic anatomy, and pathology have not been established to date (Galateanu et al. 2013). Galateanu et al. (2014) explained this by the difficulty in accessing free-ranging or captive wild animals, by their untamed disposition implying serious risks in approaching them, by the inherent risk of sedation and/or general anaesthesia, and finally by the difficulty of performing and interpreting radiographic examinations under field conditions. Additionally, the tendency of wild herbivores to hide any sign of disease until late stages can delay the realization of radiographic studies (Galateanu et al. 2014). Despite these limitations, there is an increasing interest in describing normal radiographic anatomy and radiographic protocols in the rhinoceros (Dudley et al. 2015). Fritsch et al. (2004) presented a comparative study on rhinoceros head anatomy using endoscopy, computed tomography and gross anatomy. Even though no particular results were reported regarding the ear, they reported that CT was an excellent tool for assessing the anatomic structures *in situ*. However the large size of the horn, the weight of the head and the high radiographic density of the skin complicated the procedure. A full CT examination of a white rhinoceros head is openly available online to provide basic anatomical information (WitmerLab 2012). Gerard et al. (2018) recently reported on the paranasal sinuses anatomy of the white rhinoceros using dissection and CT examination, and its clinical implication when dealing with poaching injuries.

Schellhorn (2018) presented a very interesting study looking at the potential link between lateral semicircular canal (LSC) orientation, head posture, and dietary habits in extant rhinoceroses. He used micro-computed tomography (micro-CT) of the osseous labyrinth and concluded that the inner ear provides additional information to interpret usual head postures (normal position of the head while the animal is lethargic standing or walking) linked to feeding preferences. Specifically, the white rhinoceros, a strict grazer that favours short grass, has the most downward oriented head posture when the LSCs are placed horizontally.

2.4.3 Clinical importance

From a behavioural point of view, rhinoceroses have very sharp hearing (Dinerstein 2011; Owen-Smith 2013; Vicq-D'Azyr & Cloquet 1819). Their ears swivel independently and their elongated shape allows them to detect sounds from a wide arc. They may remain alert and sensitive to the slightest sound for half an hour or longer. An erect position indicates curiosity whereas a flattened position signifies anger (Dinerstein 2011).

Clinically ears are very important as the veins of the ears are commonly and easily used to obtain blood samples and place catheters (from 20 to 16-gauge). Similarly, during general anaesthesia, the medial auricular artery is used to monitor blood pressure and draw blood gas samples (Miller & Buss 2014; Portas et al. 2006; Valverde et al. 2010; Zeiler & Stegmann 2012).

The ear pinnae are also frequently used for pulse oximeter probe placement (Miller & Buss 2014; Walzer et al. 2010).

Rhinoceros ears may play a role in heat loss, moving around continuously even when the animal is apparently sleeping (Owen-Smith 2013).

Recently a case of chronic bilateral aural hematoma in a white rhinoceros was treated by one of the senior researchers of this study (Steenkamp, Personal communication, 2017). This animal displayed an abnormal behaviour, always shaking and scratching his head and underwent a bilateral pinnectomy. There are also several reports of orphaned rhinoceros calves that have had their pinnae removed by hyaena predation after the death of their dam (Buss, Personal communication, 2018).

Ears can also display clinical signs of systemic diseases, especially in the black rhinoceros affected by superficial necrolytic dermatopathy or by idiopathic haemorrhagic vasculopathy syndrome (Miller & Buss 2014).

Ear notching is commonly used in parks and game reserves to identify populations; “V”-shaped cuts are made into the extremity of the ear to represent a number associated with the specific rhinoceros (Ngene et al. 2011). Patton (2017) also recently described the use of ear tufts to assist in the identification of individual black rhinoceroses. Once established from around 12 months of age, such tufts can easily be observed and are long-lasting. Some reserves also use ear tags to identify their rhinoceroses (Steenkamp, Personal communication, 2018).

Finally and interestingly, cases of congenital aotus (earlessness) have been reported in the black rhinoceros and were supposedly related to a sex-linked recessive gene (de Vos 1978; Goddard 1969).

CHAPTER 3: MATERIALS AND METHODS

3.1 Experimental design

Seven intact ears belonging to four southern white rhinoceroses (3 cadavers plus 1 clinical case), were used for the purpose of this descriptive study. No control group was used as this is a descriptive study. The sample size was chosen to acquire data from animals of different sexes, ages and sizes. Heads were evaluated by means of CT and computed radiography (CR) or digital radiography (DR) using the Onderstepoort Veterinary Academic Hospital (OVAH) facilities and equipment. Where possible, Magnetic Resonance Imaging (MRI) of the fresher heads was performed at a separate institution. Each study was recorded using the allocated individual's number. After completion of the imaging studies, two heads were kept in 10% formalin. Measurements of all heads and ears were taken, and the ear region was dissected in two heads. As many anatomical structures as possible were identified and labelled according to the standard international veterinary anatomical nomenclature (ICVGAN 2017). Finally micro-CT studies were performed on the caudal part of the two formalin-preserved heads.

3.2 Experimental procedures

3.2.1 Computed Tomography

The ear region of a clinical case and refrigerated heads were scanned using a dual-slice Siemens Somatom Emotion Duo CT scanner (Siemens, Germany) using the highest resolution, a pitch of 2, kernel H70s, window width (WW) of 1500 Hounsfield units (HU) and window level (WL) of 450 Hounsfield units. A Toshiba Aquilion 128 slice CT scanner (Canon Medical Systems, Japan) was used to scan one head at the Netcare Montana Hospital (Cnr Dr Swanepoel & Rooibos Streets, Montana Park, Pretoria) using a pitch of 0.656, kernel FC30, window width of 2700 Hounsfield units and window level of 350 Hounsfield units. Images were saved in DICOM format for further evaluation. Viewing and analyses was performed using RadiAnt DICOM viewer (Medixant, Poland). Measurements of the dense petrous part of the temporal bone, tympanic bulla, as well as skin thickness and external ear canal length and angle were assessed using multiplanar reconstruction.

3.2.2 Computed and Digital Radiography

A ceiling-mounted generator (APELEM Magnum VET-MT271, France), 14 X 17 inch cassettes and a CR reader (FCR XG5000 Plus, Fujifilm, Japan) or a wireless DR system (XRpad Digital X-Ray Detector, Vatex Imaging, Germany) were used to radiograph the heads. A grid was used for each radiograph (60 lines/cm; ratio 12:1; focal distance 150cm). Dorso-ventral (DV) and latero-lateral (LL) views of the ear region were made before each ear was imaged using three different obliquities (30°, 45° and 60°). A focal distance of one meter was used. Centering was done at the base of the ear close to the generator for investigation of the temporal bone. When looking at the pinna, centering was done on this structure only. Radiographic markers were used according to usual conventions. Parameters (kV and mAs) were recorded and kept as low as possible yet still producing good quality diagnostic images.

3.2.3 Magnetic Resonance Imaging

Magnetic Resonance Imaging studies were performed on the two fresher and smaller heads at the Netcare Montana Hospital using a Philips 1.5T Achieva D-stream machine (Philips, United States). Sequences used were T2W DRIVE HR transverse, T2W DRIVE HR coronal, T2W TSE* transverse, T2W TSE sagittal, FLAIR long TR* transverse and sT1W 3D HR sagittal, in accordance with protocols normally used at the Netcare Montana Hospital for evaluation of the human middle and inner ear. Data from the MRI studies will not be presented in this dissertation.

3.2.4 Anatomical dissection of the ear

Measurements were taken on all four heads using a measuring tape. Length of the head was measured from the external occipital protuberance (*Protuberantia occipitalis externa*) to the rostral aspect of the rostral horn in adults or developing horn in neonates. Width of the head was measured at its widest point, just rostral to the pinnae insertion. Length of the pinna was measured from its apex to its base. Width of the pinna was measured at its widest point, between its tragic and antitragic margins (*Margo tragicus* and *Margo antitragicus*). The two fresher heads were kept in 10% formalin and the ear region dissected in the wet skills laboratory of the OVAH. As many muscles, vessels and nerves as possible were identified, labelled according to the ICVGAN (2017) and photographs were taken.

3.2.5 Micro-CT

The formalin-preserved heads of cases 3 and 4 were transected sagittally and then transversely rostral to the ear region using a band saw. Consequently, 4 samples (left and right temporal bones of cases 3 and 4) were scanned using the micro-focus CT unit (Nikon XTH 225 ST, Nikon Metrology SARL, France) at the Micro-Focus X-ray Tomography Facility of the South African Nuclear Energy Corporation (NECSA) using 100kV and 100µA as parameters and focusing on the middle and inner ear region. Using the VGStudio Max software (Volume Graphics, Germany), tridimensional (3D) reconstructions of the middle and inner ears were obtained. Subsequently volumes of the middle ear ossicles and inner ear structures (semi-circular canals, vestibule and cochlea) were calculated.

3.3 Data analysis

Photographs obtained during dissections, radiographs, CT and micro-CT images were compared to similar images reported in domestic mammals and humans to identify and describe anatomical structures in the southern white rhinoceros.

3.4 Ethical considerations

3.4.1 Experimental animals

Heads were obtained from dead animals presented to the Pathology department or donated to us for research purpose. When clinical cases were included in this study, owner consent was obtained before doing imaging studies on the rhinoceros' head and using the results obtained from them (see Appendix A).

Approval for this study was obtained from both the Faculty Ethics Committee and the Animal Ethics Committee of the University of Pretoria (Project V088-18; see appendix B).

Permission was also obtained to do research in terms of section 20 of the animal diseases act, 1984 (ACT NO.35 of 1984). See appendix C.

3.4.2 Records

Radiographs, CT, micro-CT and MRI images as well as photographs of the dissections were stored on the personal computer of the primary investigator, as well as on an external hard drive kept by the supervisor. Data and measurements were captured in Microsoft Excel® spreadsheets, which were kept on the primary investigator's laptop.

3.4.3 Declaration of conflict of interest

None of the authors of this paper has a financial or personal relationship with other people or organisations that could inappropriately influence or bias the content of this paper.

3.5 Biosecurity and safety

The radiographic and CT examinations were performed in dedicated shielded rooms of the OVAH. No one was present in the room during image acquisition. The micro-CT unit we used at NECSA has its own shielded container preventing exposure to radiation.

Dissections were performed in the wet skills laboratory of the OVAH using protective gloves, masks and gowns. Samples were kept in 10% formalin in a well ventilated area, out of reach from other people accessing the wet skills laboratory.

CHAPTER 4: RESULTS

4.1 Study population

The study population consisted of four southern white rhinoceroses from neonatal to adult age (Table 1) with seven intact ears.

Table 1: *Population of southern white rhinoceroses used in this study showing the age of the animals used, number of intact ears per animal, as well as the different procedures that were performed on each of them.*

	Rhino 1	Rhino 2	Rhino 3	Rhino 4
Age	Adult	4 months	1 day	1 day
Intact ears	1	2	2	2
Measurements	x	x	x	x
CT	x	x	x	x
micro-CT			x	x
MRI			x	x
Radiographs	x		x	x
Dissection			x	x

The first animal (Rhino 1) was an adult cow that presented to the Pathology department at Onderstepoort after she died from anaesthetic complications. The head was handed over to us to perform imaging studies before it was opened by the pathologists. The right ear was removed during processing of the head by the pathologists.

The second animal (Rhino 2) was a juvenile bull that presented as a clinical case to the OVAH after being attacked by predators, likely lions, in his left elbow region. As the animal was already anesthetised in the CT room to scan his elbow, he was included in our study after obtaining owner's consent. After treatment at the OVAH, this animal was discharged and therefore no dissection studies were performed.

Finally, two 1-day old southern white rhinoceros heads were donated to us by a rhinoceros breeding farm. One of the rhinoceros calves drowned (Rhino 3) and the other was trampled to death (Rhino 4).

4.2 Morphometry of the head and pinnae

The length and width of the heads and pinnae were measured on all four southern white rhinoceroses included in this study population (Table 2).

Table 2: *Dimensions of the head and pinnae of the study population of southern white rhinoceroses.*

	Rhino 1		Rhino 2		Rhino 3		Rhino 4	
Age	Adult		4 months		1 day		1 day	
Head length (cm)	80		40		30		35	
Head width (cm)	40		26		15		18	
	Left	Right	Left	Right	Left	Right	Left	Right
Pinna length (cm)	30	missing	22	22	15	15	15	15
Pinna width (cm)	20	missing	14	14	10	10	12	12

Not surprisingly, the dimensions of the left and right pinnae from the same animal were similar. Roughly, the pinna of a neonate is twice as small as its adult counterpart.

4.3 Anatomical dissection of the ear

Dissection of the ear region could only be performed on the two neonates (Rhinos 3 and 4).

4.3.1 Cartilages of the ear

Similar to what is described in horses (Barone 2010b; Collin 2006), three pieces of cartilage compose the external ear of the southern white rhinoceros: the scutiform cartilage (*cartilago scutiformis*), the auricular cartilage (*cartilago auriculae*) and the annular cartilage (*cartilago anularis*).

4.3.1.1 Scutiform cartilage

The scutiform cartilage appears as a roughly isosceles triangular cartilaginous plate with a dorsal base and a ventral apex. It is located rostro-medially to the pinna at the surface of the temporal muscle (Figures 3 to 5). On Rhino 3, its long axis was 7cm long and its short axis was 4.5cm wide. It gives insertion to 5 muscles (see next section – 4.3.2 Myology).

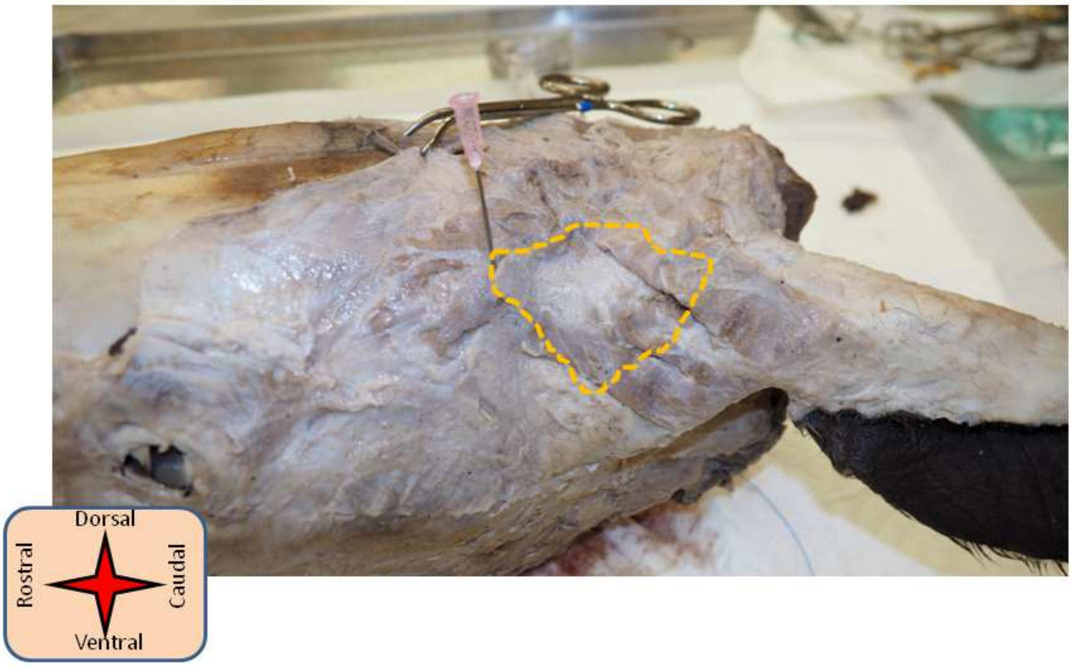

Figure 3: Position of the left scutiform cartilage is outlined by an orange dashed line after skin removal only. Rhino 3.

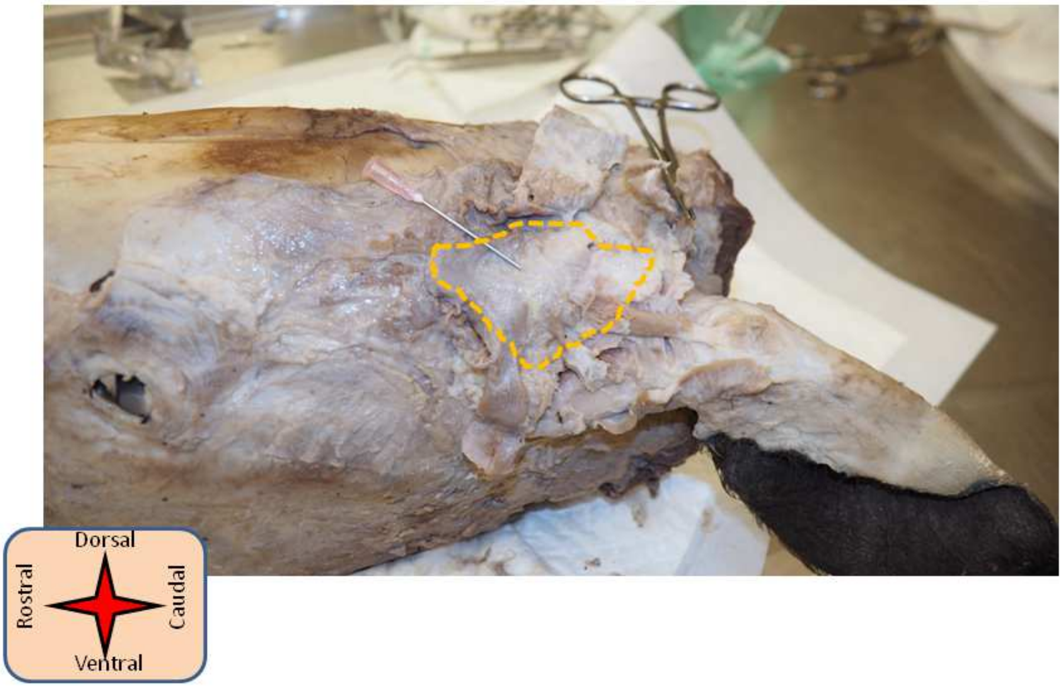

Figure 4: Position of the left scutiform cartilage is outlined by an orange dashed line after removal of *mm. scutuloauricularis superficialis dorsalis, medius and ventralis.* Rhino 3.

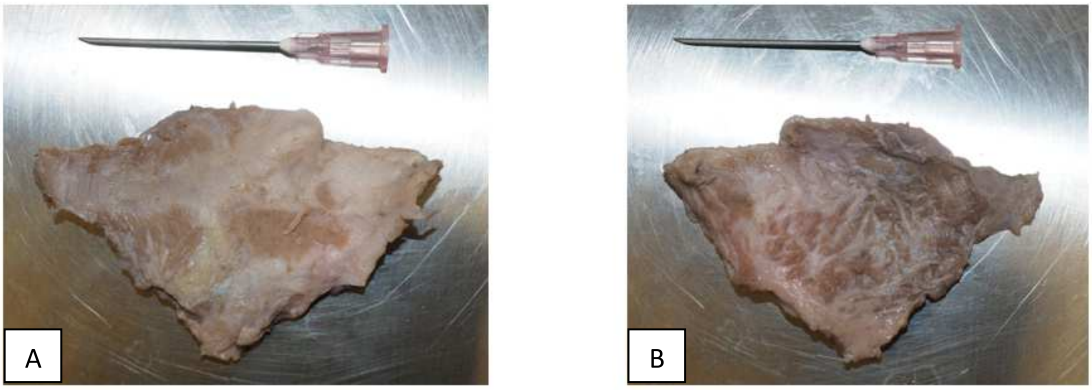

Figure 5: Lateral (A) and medial (B) views of the left scutiform cartilage. Rhino 3.

4.3.1.2 Auricular cartilage

The auricular cartilage is a thin blade of elastic cartilage rolled on itself. It is a major component of the external ear canal (*meatus acusticus externus*) and forms the pinna opening rostro-laterally. It is covered with a very thin adherent skin and provides insertion to 6 or 7 muscles (see next section – 4.3.2 Myology). The intertragic notch (*incisura intertragica)* is visible at the entrance of the external ear canal (Figure 6). The latter lies on the temporal muscle on which it can move thanks to a small fat pad (Figure 7). Rostro-laterally, the external ear canal is covered by the triangular parotid gland and seems to be attached to the zygomatic arch of the temporal bone by a band of fibrous tissue (Figure 8). Once isolated, the styloid process (*processus styloideus*) of the auricular cartilage is visible, pointing ventrally and overlying the lateral aspect of the annular cartilage (Figure 9).

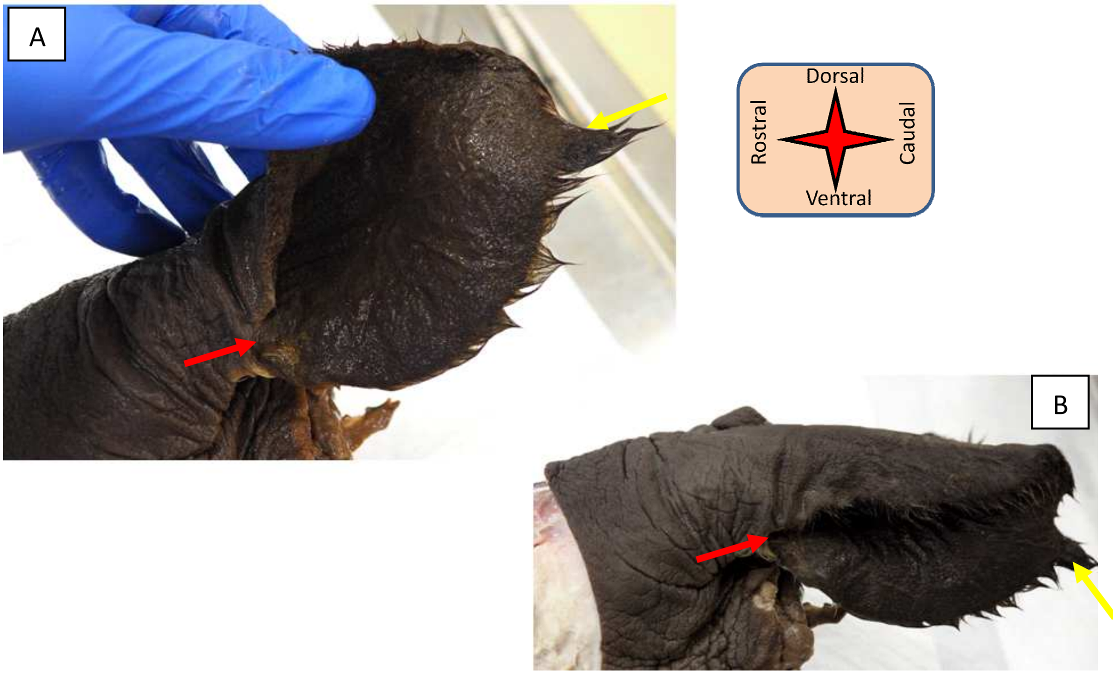

Figure 6: Open (A) and closed resting (B) views of the left auricular cartilage in place. Its apex (yellow arrow) and intertragic notch (red arrow) are visible. Obtained from Rhino 3.

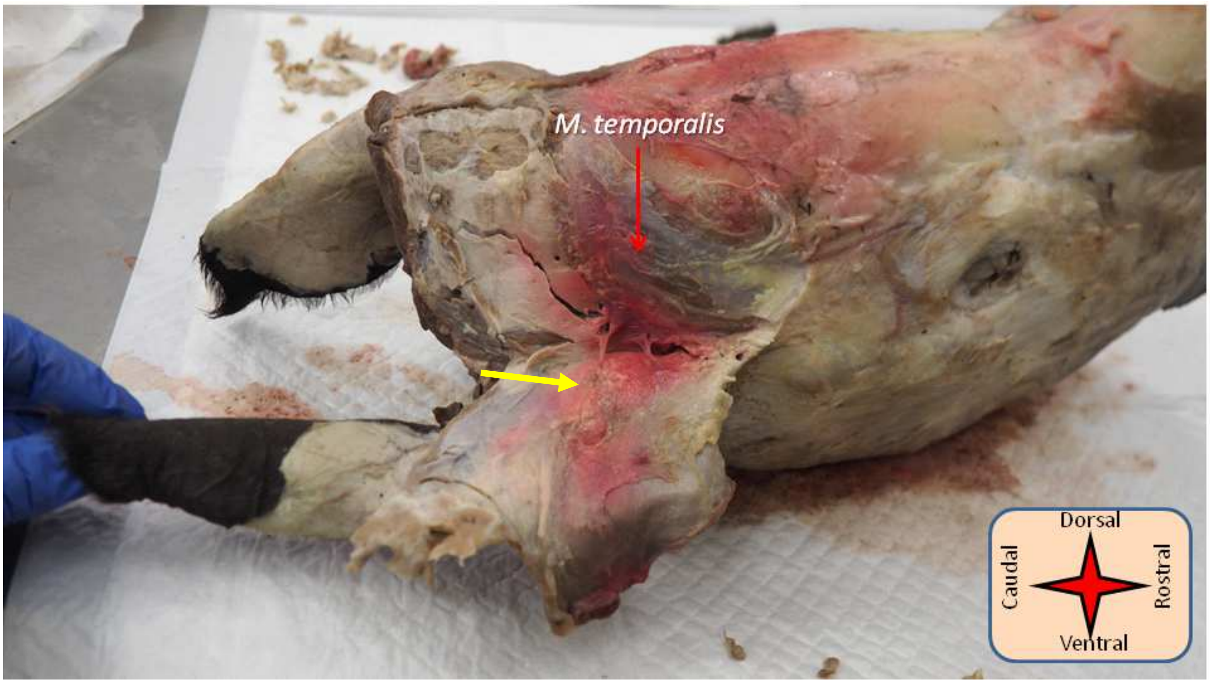

Figure 7: The external ear canal retracted from the temporal muscle (red arrow). The small fat pad allowing movement of the pinna is visible (yellow arrow). Obtained from the right side of Rhino 3.

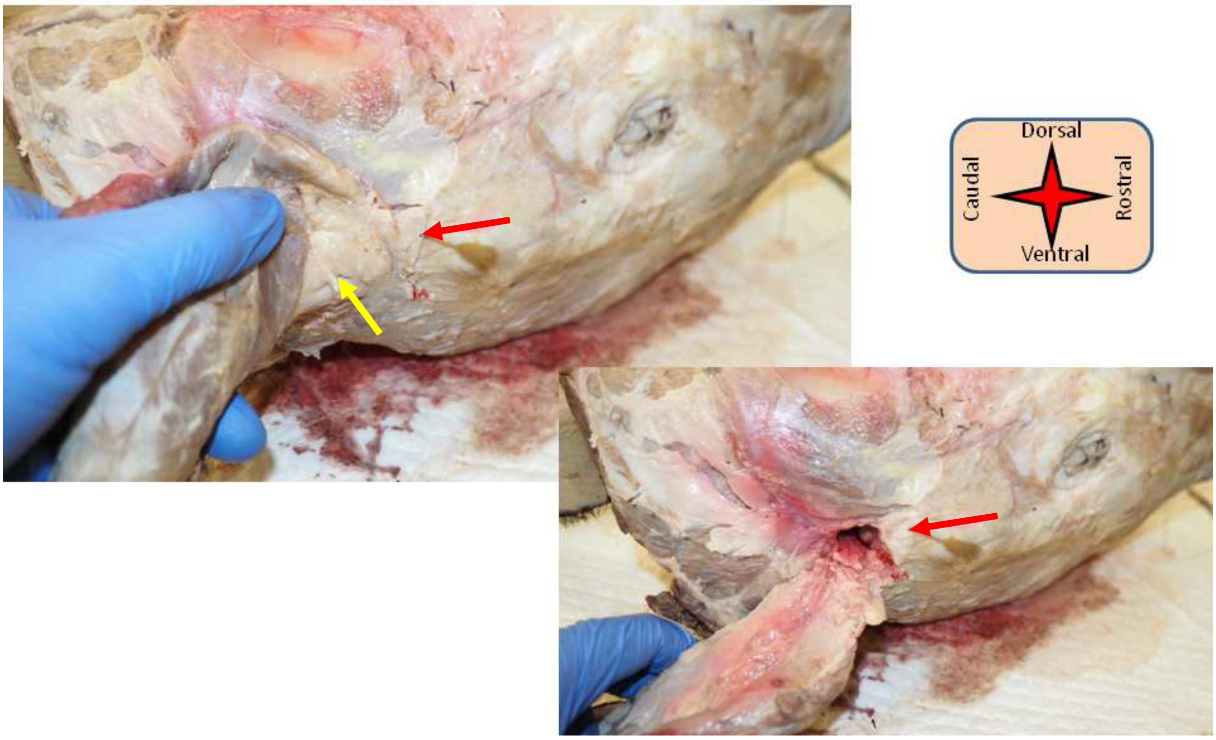

Figure 8: The attachment of the external ear canal to the zygomatic arch is highlighted (red arrow), as well as the parotid gland (yellow arrow). Obtained from the right side of Rhino 3.

4.3.1.3 Annular cartilage

The annular cartilage is a small cartilage plate rolled on itself into a tube. It is also a part of the external ear canal (*meatus acusticus externus*)(Figures 9 and 10). It embraces the bony *porus acusticus externus* proximally and is connected to the auricular cartilage by an elastic membrane distally. On Rhino 3, its long axis was 4cm long.

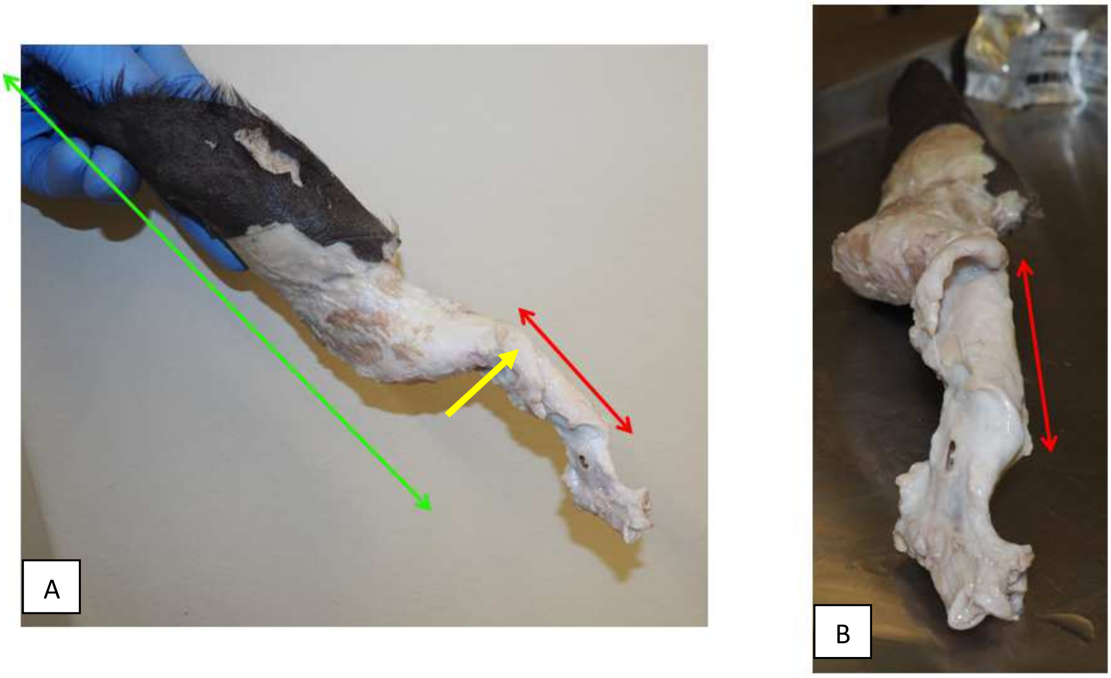

Figure 9: Caudal (A) and proximal (B) views of the isolated right cartilaginous external ear canal. The lengths of the auricular cartilage and annular cartilage are highlighted by the green and red double-headed arrows, respectively. The styloid process of the auricular cartilage is highlighted by the yellow arrow. Obtained from Rhino 3.

Figure 10: Open (A) and transverse (B) views of the isolated cartilaginous right external ear canal. The length of the annular cartilage is highlighted by the red double-headed arrow. Obtained from Rhino 3.

4.3.2 Myology

Very thin intrinsic auricular muscles are found on the auricular and annular cartilages. These are responsible for the tonicity of the external ear. No further detail will be given here.

This study mainly focuses on the extrinsic auricular muscles. These originate on bones or fascia of the head or neck and end on the cartilages of the external ear. Alternatively they sometimes connect the cartilages of the ear. They are typically separated into four groups (Barone 2010b):

4.3.2.1 Rostral auricular muscles (*Mm. auriculares rostrales*)

4.3.2.1.1 M. zygomaticoauricularis

The presence of this muscle, that pulls the ear rostrally in the horse and brings the opening of the pinna forward, could not be confirmed on any of the dissected specimen.

4.3.2.1.2 M. zygomaticoscutularis

Despite its name, this muscle does not seem to reach the zygomatic arch but instead inserts on the frontal bone and orbital ligament. Caudally it reaches the rostral and lateral part of the scutiform cartilage (Figure 11). It pulls the scutiform cartilage in rostral and lateral directions.

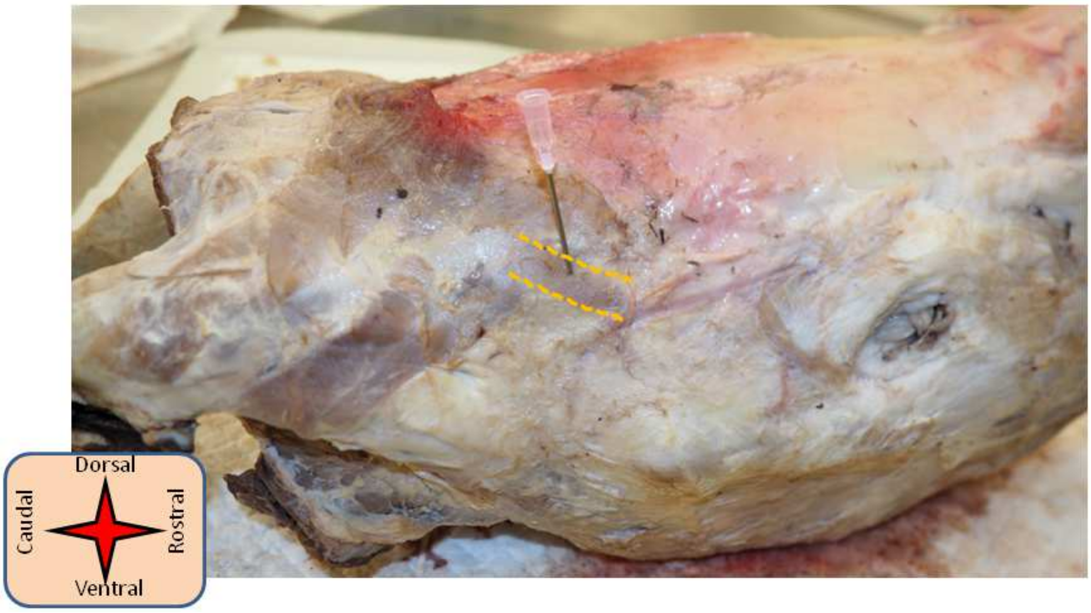

Figure 11: Lateral view highlighting the right *m. zygomaticoscutularis* (orange dashed lines). Obtained from Rhino 3.

4.3.2.1.3 M. frontoscutularis

Located more dorsally than the previous muscle, it runs from the frontal bone, next to the temporal line, up to the rostro-medial border of the scutiform cartilage (Figure 12). It pulls the scutiform cartilage in rostral direction and thereby also the pinna.

Figure 12: Lateral view highlighting the left *m. frontoscutularis* (orange dashed lines). Obtained from Rhino 3.

4.3.2.1.4 Mm. scutuloauriculares superficiales

Like in horses, four *mm. scutuloauriculares superficiales* can be identified in the southern white rhinoceros: *dorsalis, medius, ventralis* and *accessorius*. They all run between the superficial part of the scutiform cartilage and the base of the auricular cartilage (Figures 13 and 14). The *m. accessorius* runs obliquely under the *m. scutuloauricularis superficialis dorsalis* and tends to rotate the pinna laterally. The other three muscles pull the pinna rostrally and medially. The *m. scutuloauricularis superficialis dorsalis* is continuous dorsally with the *m. interscutularis*, similar to that of the horse (Barone 2010b).

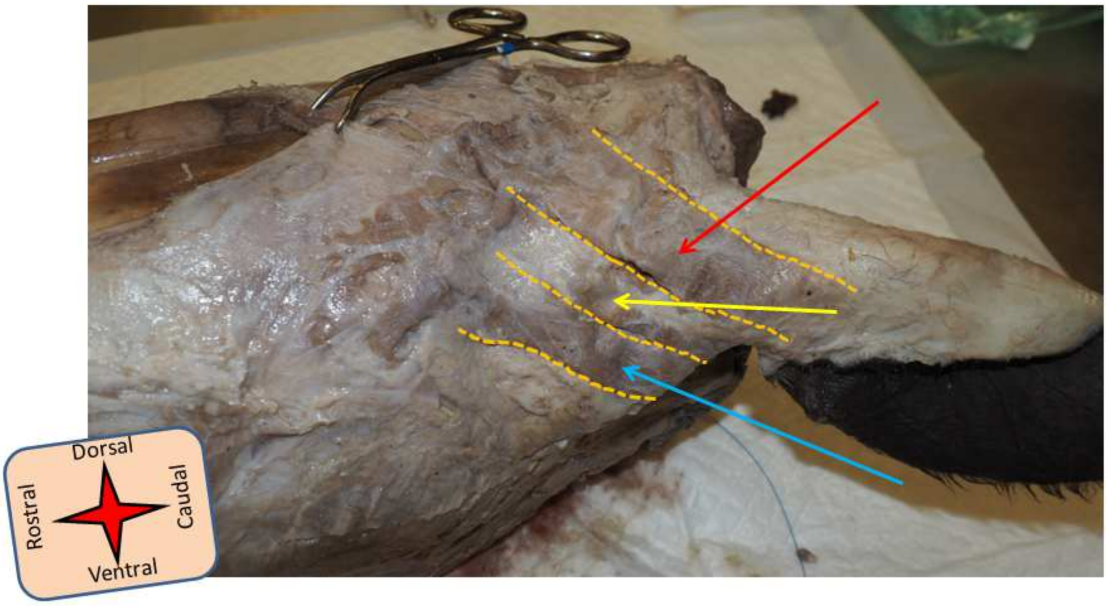

Figure 13: Lateral view highlighting the left *mm. scutuloauriculares superficiales* (orange dashed lines). The red arrow points to the *dorsalis*.The yellow arrow highlights the *medius*. The blue arrow points to the *ventralis*. The *accessorius* one is hidden under the *dorsalis*. Obtained from Rhino 3.

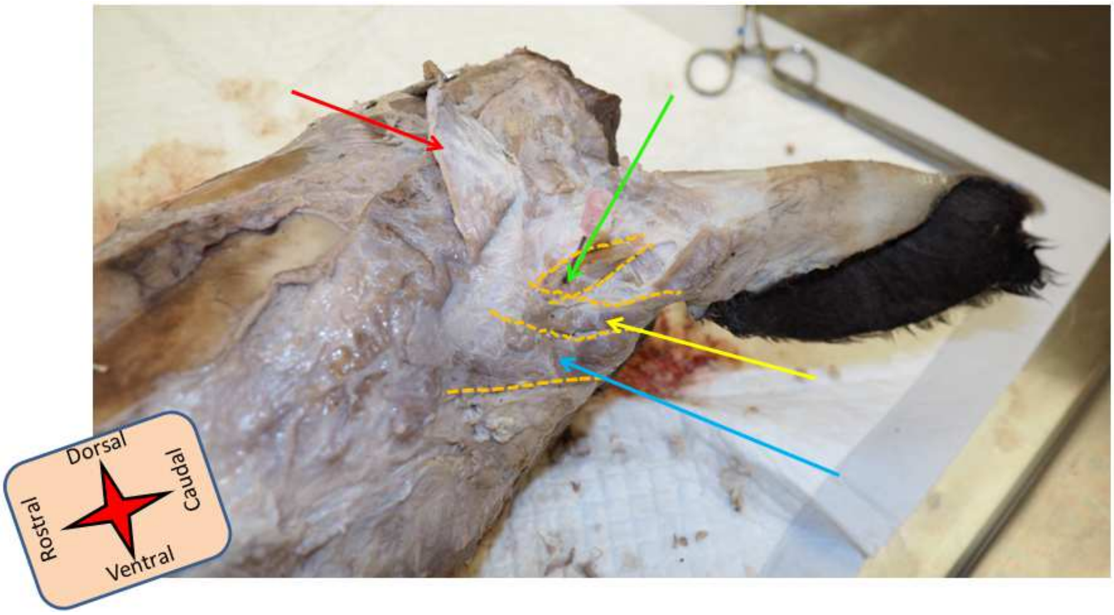

Figure 14: Lateral view highlighting the left *mm. scutuloauriculares superficiales* (orange dashed lines). The green arrow points to the *accessorius*. The yellow arrow highlights the *medius*. The blue arrow points to the *ventralis*. The *dorsalis* is reflected dorsally (red arrow). Obtained from Rhino 3.

4.3.2.1.5 Mm. scutuloauriculares profundi

Two deep scutoloauricular muscles were observed: the *m. scutuloauricularis profundus major* and the *m. scutuloauricularis profundus minor.* The *minor* inserts on the caudo-medial angle of the scutiform cartilage whereas the *major* inserts more centrally under this cartilage, superficial to the temporal fascia (Figures 15 and 16). Both join the base of the pinna deep to the *mm. scutuloauriculares superficiales*. They are likely to rotate the pinna medially.

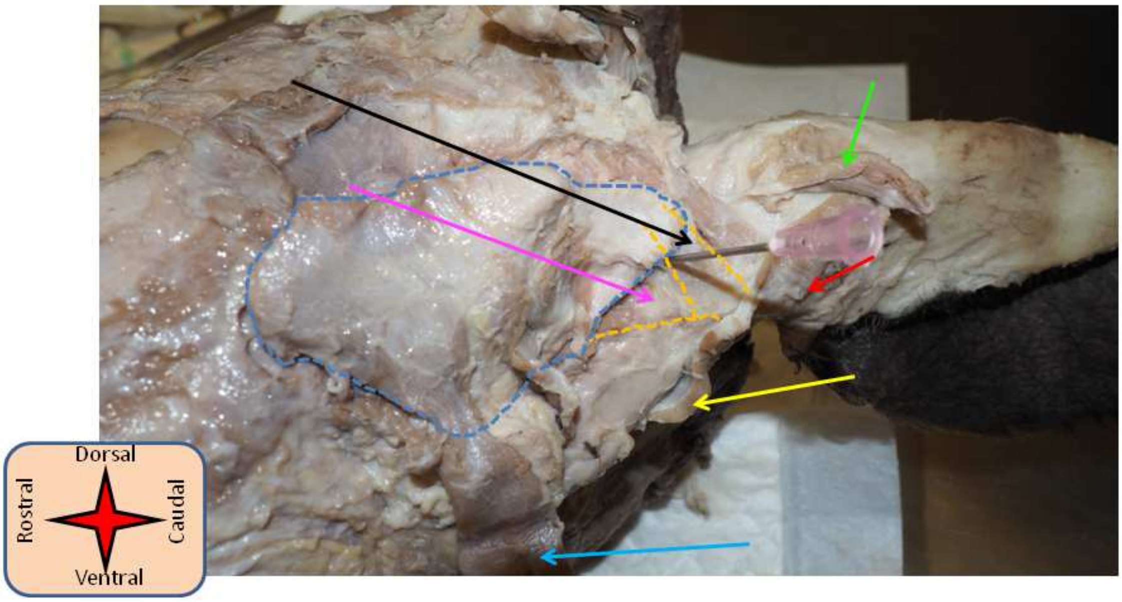

Figure 15: Lateral view highlighting the left *mm. scutuloauriculares profundi* (orange dashed lines). Black arrow: *m. scutuloauricularis profundus minor*; pink arrow: *m. scutuloauricularis profundus major*; green arrow: *m. scutuloauricularis superficialis accessorius*; yellow arrow: *medius*; blue arrow: *ventralis*; red arrow: *dorsalis*. The margins of the scutiform cartilage are highlighted (blue dashed line). Obtained from Rhino 3.

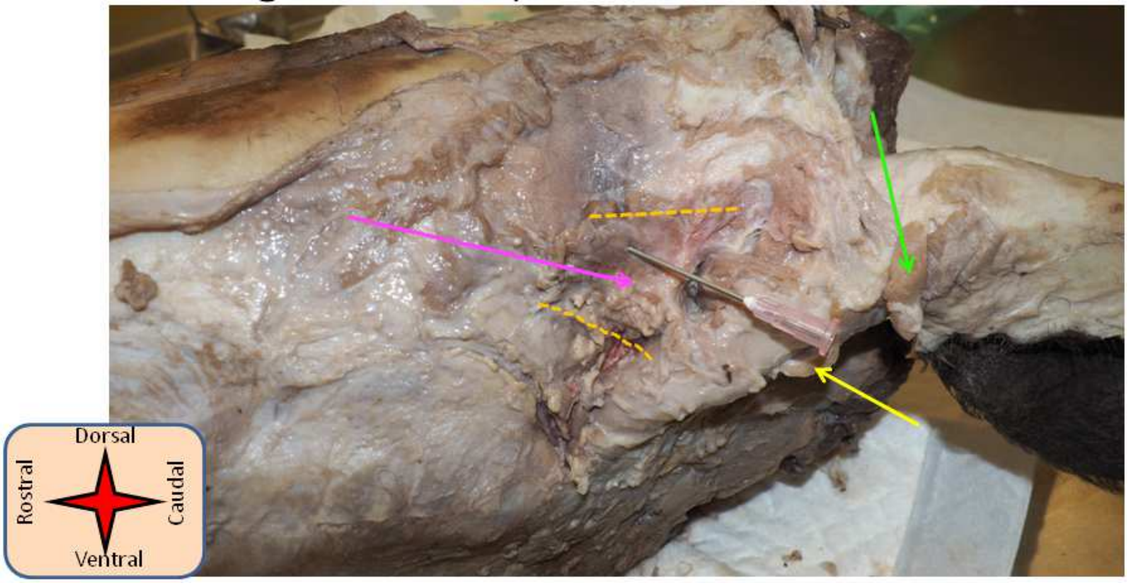

Figure 16: Lateral view highlighting the left *m. scutuloauriculares profundi major* (orange dashed lines and pink arrow) after removal of the scutiform cartilage. Green arrow: *m. scutuloauricularis superficialis accessorius*; yellow arrow: *medius*. Obtained from Rhino 3.

4.3.2.2 Dorsal auricular muscles (*Mm. auriculares dorsales*)

4.3.2.2.1 M. interscutularis

This muscle appears as an unpaired transverse band covering the frontal bones, without an obvious median raphe, inserting on the dorso-medial aspect of the scutiform cartilage. Its most caudal fibers seems to be continuous with the *m. scutuloauricularis superficialis dorsalis* (Figure 17). It pulls both scutiform cartilages towards the median plane and rotates the pinnae medially.

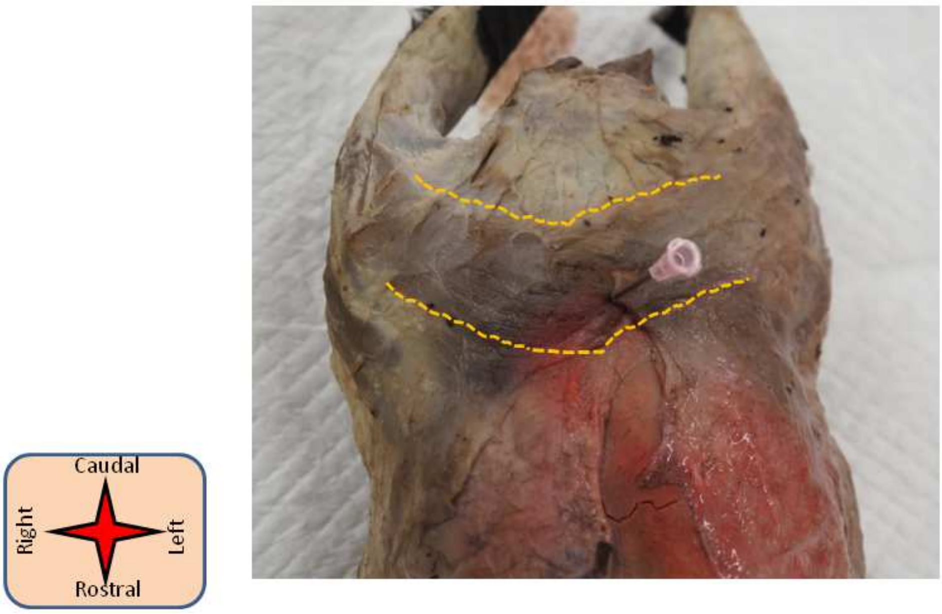

Figure 17: Dorsal view highlighting the *m. interscutularis* (orange dashed lines). Obtained from Rhino 3.

4.3.2.2.2 M. parietoauricularis

This muscle is partially hidden by the *mm. interscutularis*, *scutuloauricularis superficialis dorsalis* and the *cervicoscutularis*. It runs between the caudal part of the parietal bone and the caudo-medial pinna (Figure 18). It raises the pinna and rotates it medially.

Figure 18: Dorso-lateral view highlighting the right *m. parietoauricularis* (orange dashed lines). Obtained from Rhino 3.

4.3.2.2.3 M. parietoscutularis

It is only described in the rabbit, ruminants and carnivores as a rostral branch of the previous muscle (Barone 2010b). It was not observed in the southern white rhinoceros.

4.3.2.3 Caudal auricular muscles (*Mm. auriculares caudales*)

4.3.2.3.1 M. cervicoscutularis

The caudal part is visible, inserting on the nuchal ligament, but rostrally it runs under the *m. scutuloauricularis superficialis dorsalis* before reaching the caudal margin of the scutiform cartilage (Figure 19). It pulls the scutiform cartilage medially and in doing so straightens the ear.

Figure 19: Dorso-lateral view highlighting the right *m. cervicoscutularis* (orange dashed lines). Obtained from Rhino 3.

4.3.2.3.2 M. cervicoauricularis superficialis

This muscle runs rostro-laterally between the nuchal ligament, close to the external occipital protuberance, and the medial part of the pinna (Figure 20). It pulls the pinna in a caudo-medial direction and raises it.

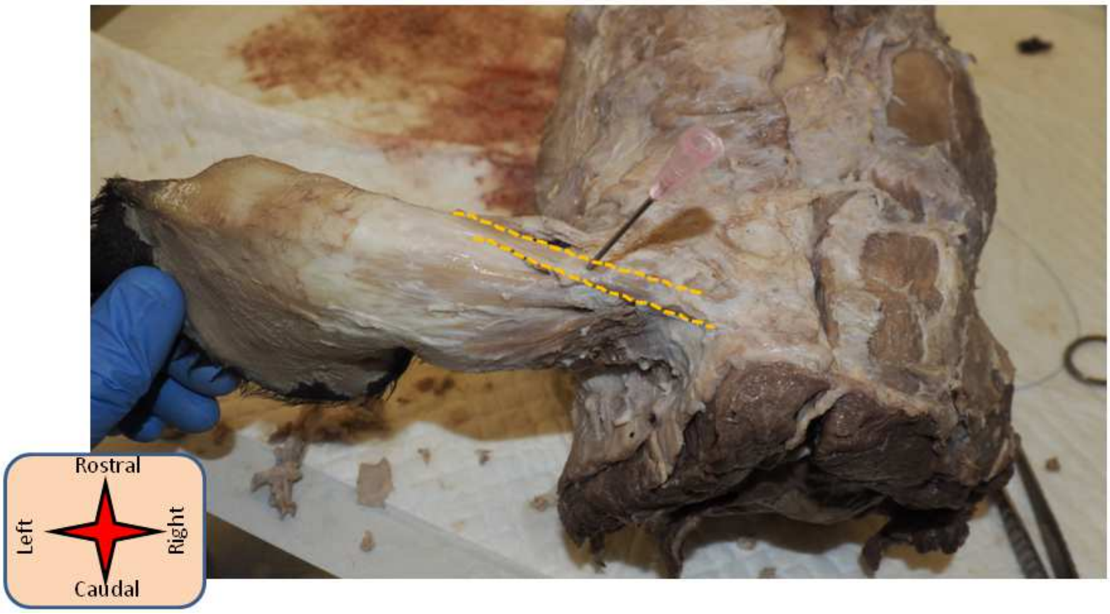

Figure 20: Dorsal view highlighting the left *m. cervicoauricularis superficialis* (orange dashed lines). Obtained from Rhino 3.

4.3.2.3.3 M. cervicoauricularis medius

This muscle inserts on the nuchal ligament, close to the external occipital protuberance and reaches the ventral commissure of the pinna, adjacent to the *m. parotidoauricularis* (Figure 21). It pulls the pinna in a caudal direction, bringing its opening laterally and caudally.

Figure 21: Caudal view highlighting the left *m. cervicoauricularis medius* (orange dashed lines). Obtained from Rhino 3.

4.3.2.3.4 M. cervicoauricularis profundus

Its medial insertion is similar but deeper than the previous two muscles. It joins the caudo-lateral base of the pinna (Figure 22). It shares the action of the previous muscle.

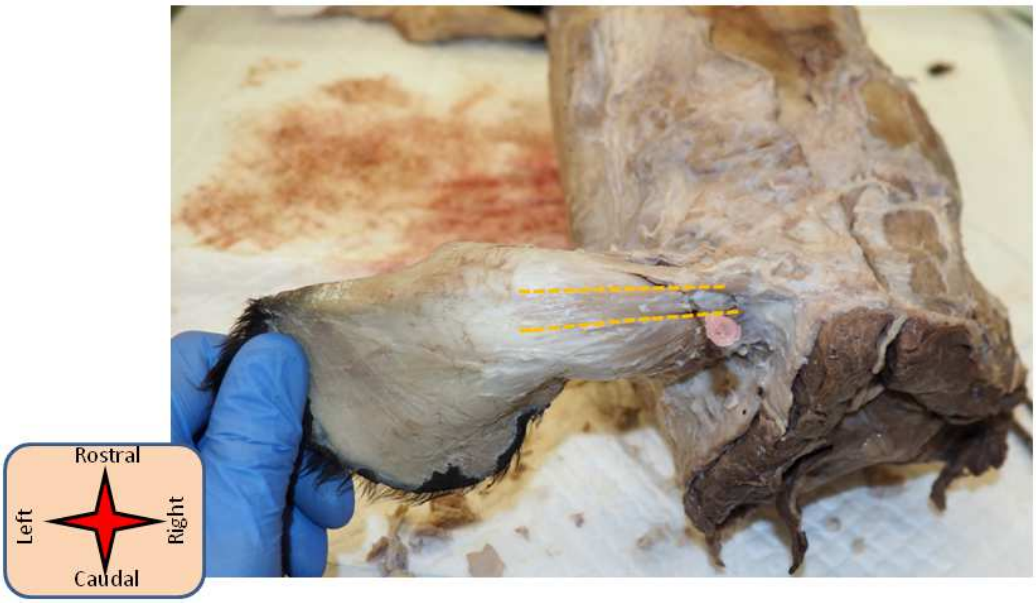

Figure 22: Caudal view highlighting the left *m. cervicoauricularis profundus* (orange dashed lines). Obtained from Rhino 3.

4.3.2.4 Ventral auricular muscles (*Mm. auriculares ventrales*)

4.3.2.4.1 M. parotidoauricularis

This muscle runs superficial to the parotid gland and inserts at the base of the auricular cartilage laterally (Figure 23). It lowers and abducts the pinna.

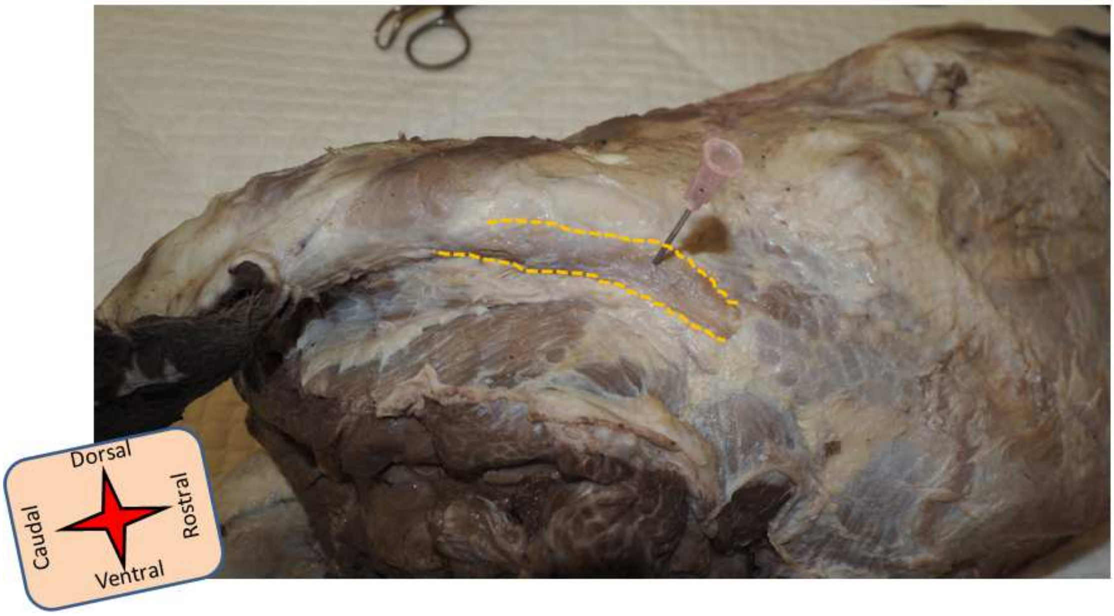

Figure 23: Lateral view highlighting the right *m. parotidoauricularis* (orange dashed lines). Obtained from Rhino 4.

4.3.2.4.2 M. styloauricularis

It inserts on the temporal bone, ventrally to the *porus acusticus externus* and ends at the medial aspect of the base of the auricular cartilage. It is covered by the parotid gland and the rostral auricular muscles (Figure 24). In the horse it supposedly shortens the tubular portion of the external ear but seems to induce medial rotation of the pinna in the rhinoceros.

Figure 24: Lateral view highlighting the left *m. styloauricularis* (orange dashed lines). Obtained from Rhino 3.

4.3.3 Angiology

The arterial and venous supply to the ear is described on macroscopic dissection only, no plastination studies were done. The main arterial branches coming from the external carotid artery (*arteria carotis externa*) were isolated in the ear region.

Caudally to the pinna, the caudal auricular artery (*a. auricularis caudalis*) emerges from the caudal part of the external carotid artery (Figure 25). It then runs dorsally under the parotid gland and caudal to the *m. parotidoauricularis*. It gives rise to muscular and parotidian rami.

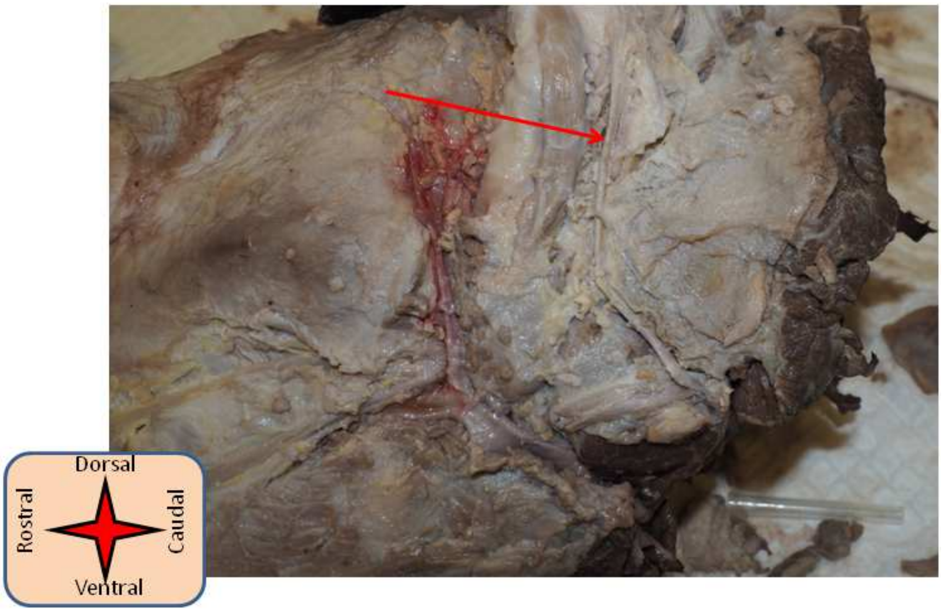

Figure 25: Lateral view highlighting the left caudal auricular artery (red arrow). Obtained from Rhino 3.

The deep auricular artery (*a. auricularis profunda*) emerges from the maxillary artery medially to the base of the pinna and provides muscular rami before going through the caudal aspect of the auricular cartilage (Figure 26).

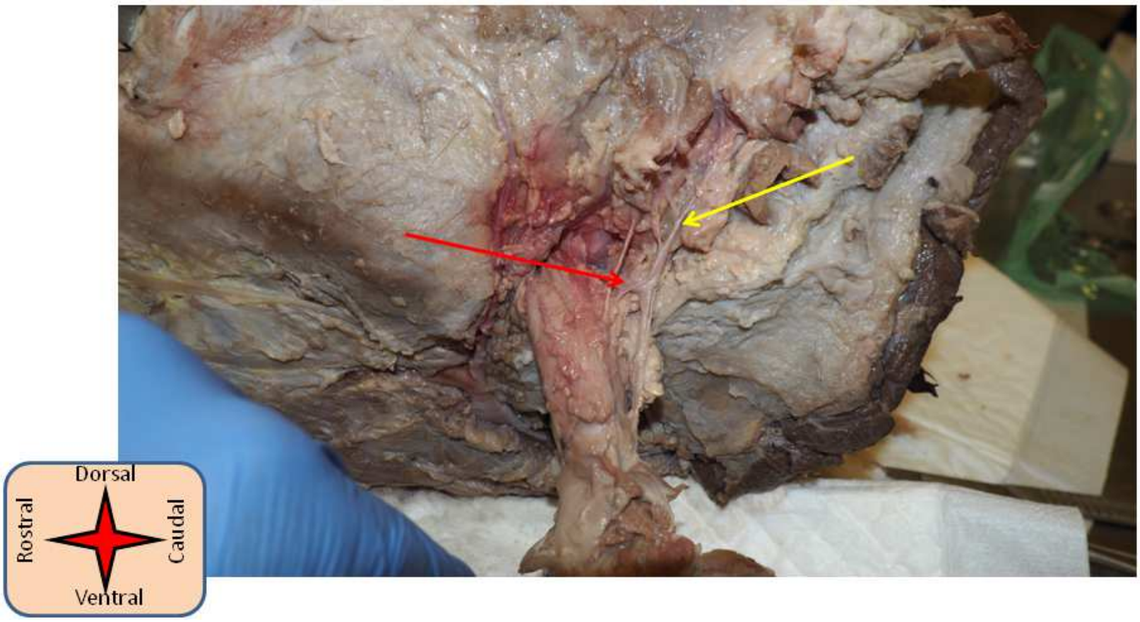

Figure 26: Dorso-lateral view highlighting the left deep auricular artery (red arrow) and its branches. Yellow arrow: muscular rami. Obtained from Rhino 3 after elevation of the pinna.

Rostrally to the pinna, the rostral auricular artery (*a. auricularis caudalis*) emerges from the external carotid artery at the same level as the superficial temporal artery (*a. temporalis superficialis*) just caudal to the temporomandibular joint, below the parotid gland (Figure 27). It then runs between the base of the pinna and the temporal muscle.

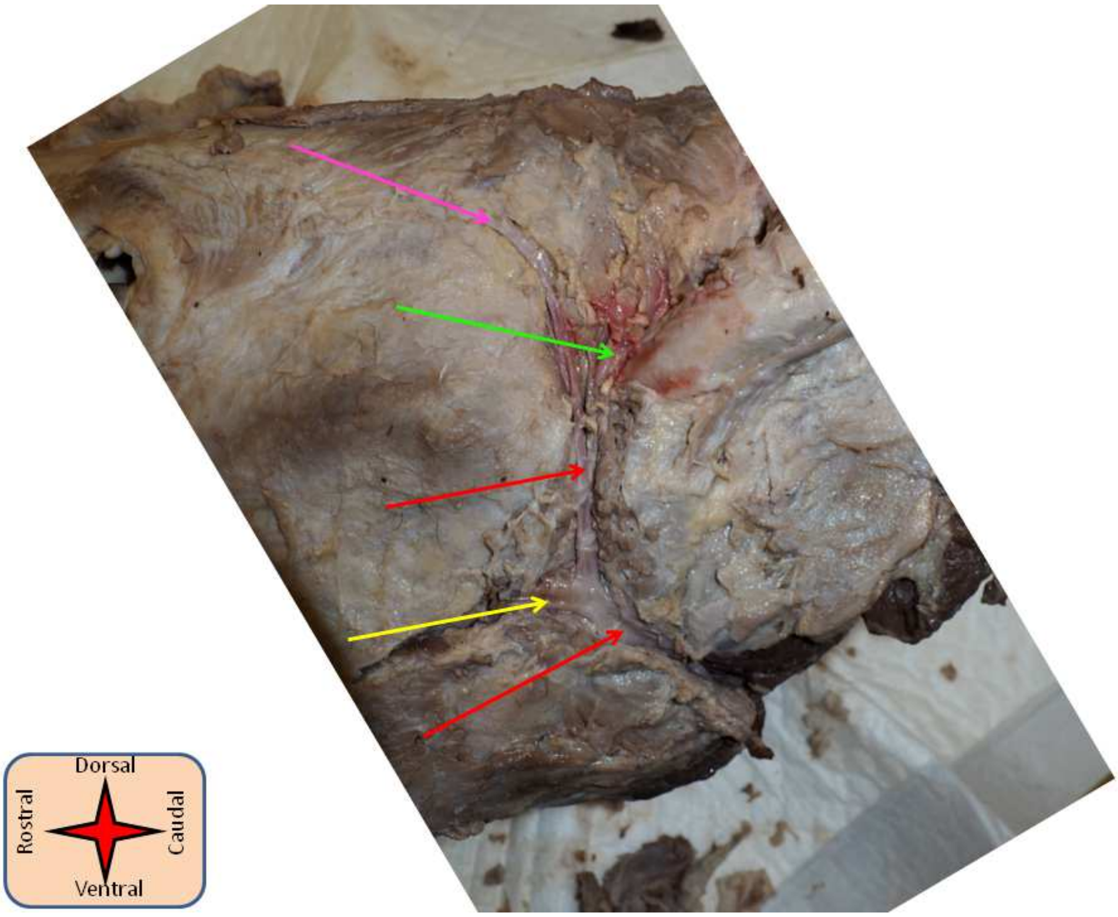

Figure 27: Lateral view highlighting the branches of the left external carotid artery (red arrow) and the rostral auricular blood supply. Yellow arrow: linguofacial trunk; green arrow: rostral auricular artery; pink arrow: superficial temporal artery. Obtained from Rhino 3.

The disposition of the auricular veins has not been described in detail. Only the rostral and caudal auricular veins (*v. auricularis rostralis* and *caudalis*) were observed upon removal of the thin skin covering the auricular cartilage. The caudal auricular vein has a Y shape. One branch of the Y is directed toward the apex of the pinna whereas the other reaches the antitragic margin of the pinna (Figure 28). Its rostral counterpart also has 2 branches: one reaching the tragic margin of the pinna and the other reaching the ventral commissure of the pinna (Figure 29).

Figure 28: Caudal view highlighting the two branches of the right caudal auricular vein (red arrow). Obtained from Rhino 3.

Figure 29: Lateral view highlighting the two branches of the right rostral auricular vein (red arrow). Obtained from Rhino 3.

4.3.4 Neurology

The facial nerve (*n. facialis*) was clearly seen emerging ventral to the osseous external ear canal. Its buccal rami (*rami buccales*) were observed rostrally at the surface of the masseter muscle (Figure 30). However, it was difficult to isolate the fine branches of the facial nerve responsible for the innervation of the external ear.

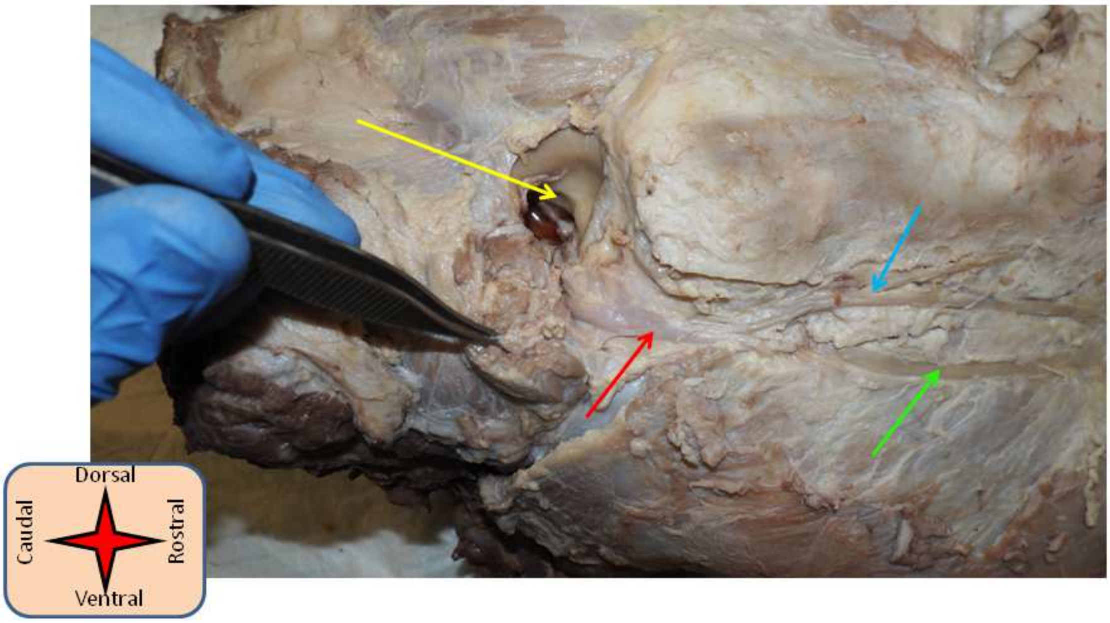

Figure 30: Lateral view highlighting the right facial nerve (red arrow). Yellow arrow: osseous external ear canal; blue arrow: *ramus dorsalis buccalis*; green arrow: *ramus ventralis buccalis*. Obtained from Rhino 3.

4.3.5 Eustachian tube

The Eustachian tube, also known as the auditory or pharyngotympanic tube, or *tuba auditiva*, was observed during our dissections, particularly after sectioning of the heads. The *ostium pharyngeum tubae auditivae* was clearly visible on the lateral wall of the nasopharynx, about 3mm wide. It was open without an obvious mucosal elevation or cartilaginous flap (Figure 31).

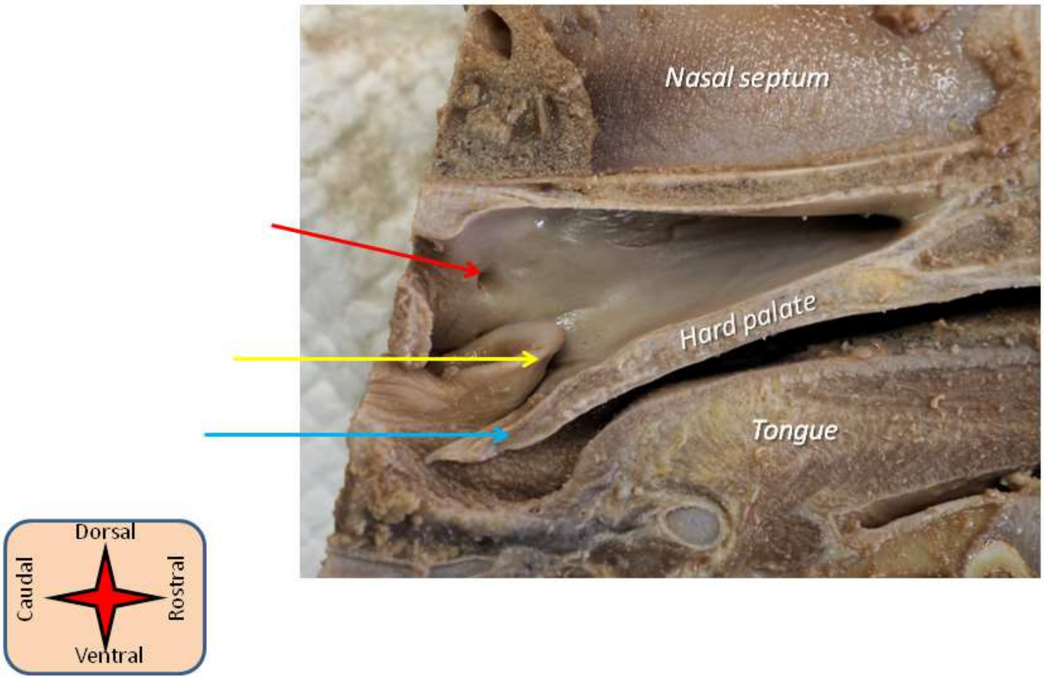

Figure 31: Medial view obtained from the left side of Rhino 3 after sagittal sectioning of its head. The pharyngeal opening of the auditory tube (*ostium pharyngeum tubae auditivae*) is visible (red arrow) on the lateral wall of the nasopharynx. Yellow arrow: epiglottis; blue arrow: soft palate.

It was possible to catheterize the Eustachian tube to follow the path of the cartilaginous auditory tube along the dorso-lateral wall of the epipharyngeal bursa for 10cm in Rhino 3 (representing 1/3 of the total head length) (Figure 32). The opening of the auditory tube in the middle ear at the level of the tympanic bulla could be observed on a transverse head section (Figure 33).

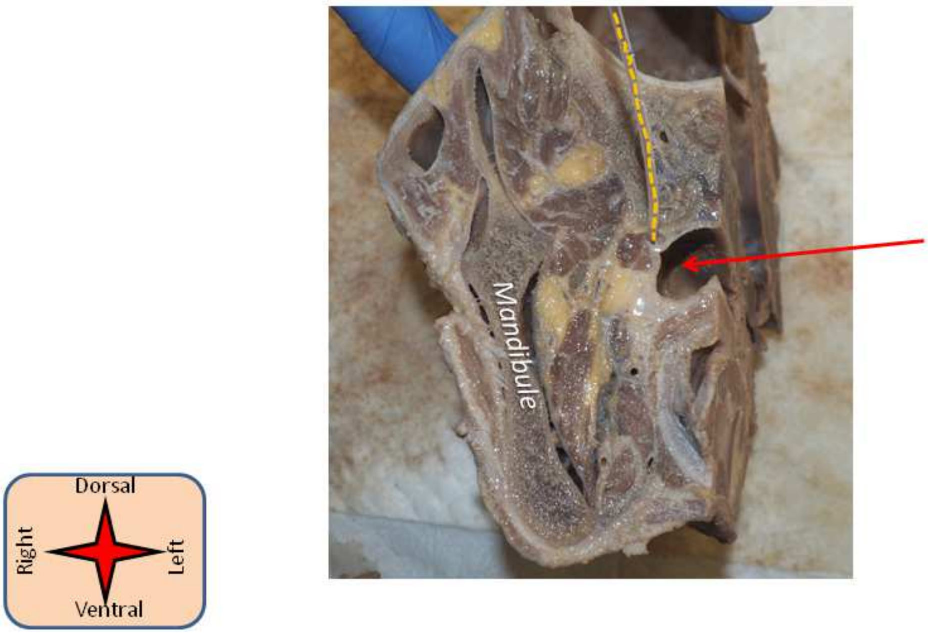

Figure 32: Rostral view obtained from the right side of Rhino 3 after transverse sectioning of its head caudal to the larynx. The path of the catheterized auditory tube is visible dorso-laterally to the epipharyngeal bursa (red arrow). The catheter is highlighted by the orange dashed line.

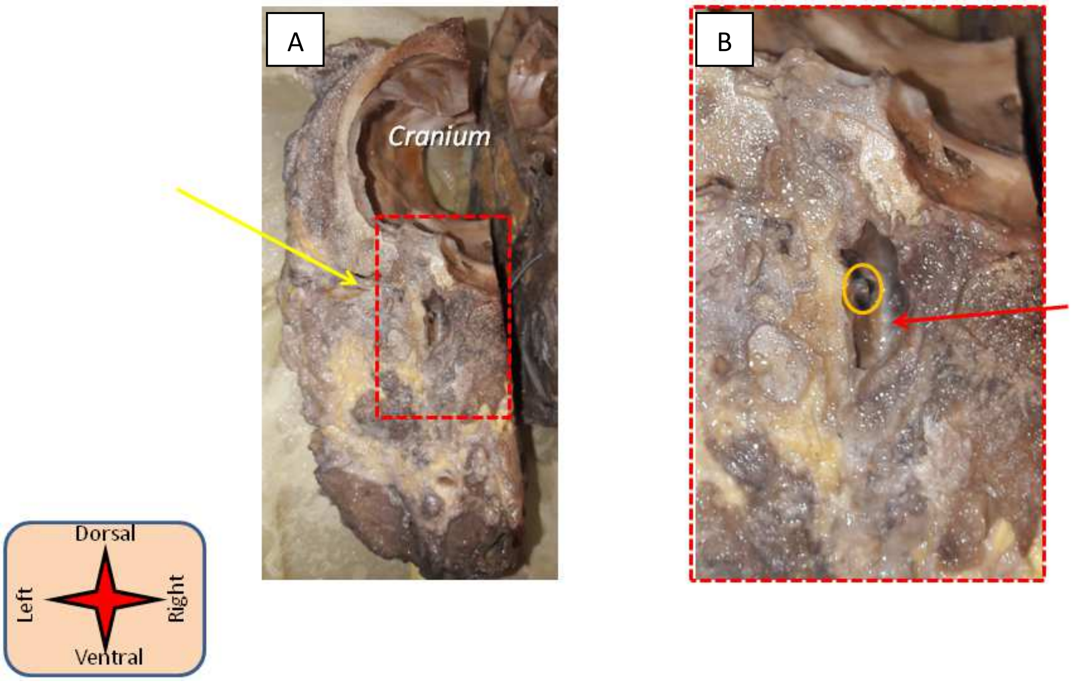

Figure 33: Caudal view obtained from the left side of Rhino 3 after transverse sectioning of its head at the tympanic bulla's level (red arrow). The opening of the catheterized auditory tube is visible in the bulla. A: Full view; B: Close up. The catheter tip is highlighted by the orange oval line. Yellow arrow: external acoustic meatus.

4.4 Radiographic anatomy of the ear

The fresh heads of Rhinos 1, 3 and 4 were radiographed (Table 3).

Table 3: *Radiographic equipment and parameters used in this study on three southern white rhinoceroses' heads.CR: Computed Radiography; DR: Digital Radiography; DV: Dorso-Ventral; LL: Latero-lateral.*

	Rhino 1		Rhino 3		Rhino 4	
Equipment	CR		DR		DR	
	kV	mAs	kV	mAs	kV	mAs
DV	120	80	90	20	90	20
LL	100	80	90	20	90	20
Obliques	100	80	90	20	90	20
Pinna	60	6.3	50	4	50	4

Radiographic examination of the ear of the adult southern white rhinoceros (Rhino 1) was challenging. The outline of the skull was visible, mainly thanks to the large air-filled sinuses, but superimposition, thickness of the head and soft tissue, as well as some fluid lines in the sinuses made assessment of the different bony structures tedious (Figures 34 to 37). The margins of the external ear canal were also difficult to visualize.

On the LL view, the external acoustic meatus was visible and the position of the petrous part of the temporal bone could roughly be identified (Figure 34). The 30°Dorsal to Ventral Oblique view allowed a better identification of this latter structure on the contralateral side but overall the contrast remained poor (Figure 35). On the 45°Dorsal to Ventral Oblique view, it was superimposed on the caudal aspect of the dorsal cranium. On the 60°Dorsal to Ventral Oblique view, it was visible but affected by distortion. Additionally the image had a poor contrast and only the most dorsal structures of the head were visible (Figure 36). On the DV view, some bony outlines could be identified but accurate identification of the ear-related structures was also difficult, with a poor contrast (Figure 37). A dog naso-gastric tube was inserted in the external ear canal in some of these radiographs. Metallic markers at its distal extremity helped in localizing the ear-related structures.

When focusing on the pinna, a very good contrast could be obtained and the shape of the auricular cartilage was visible.

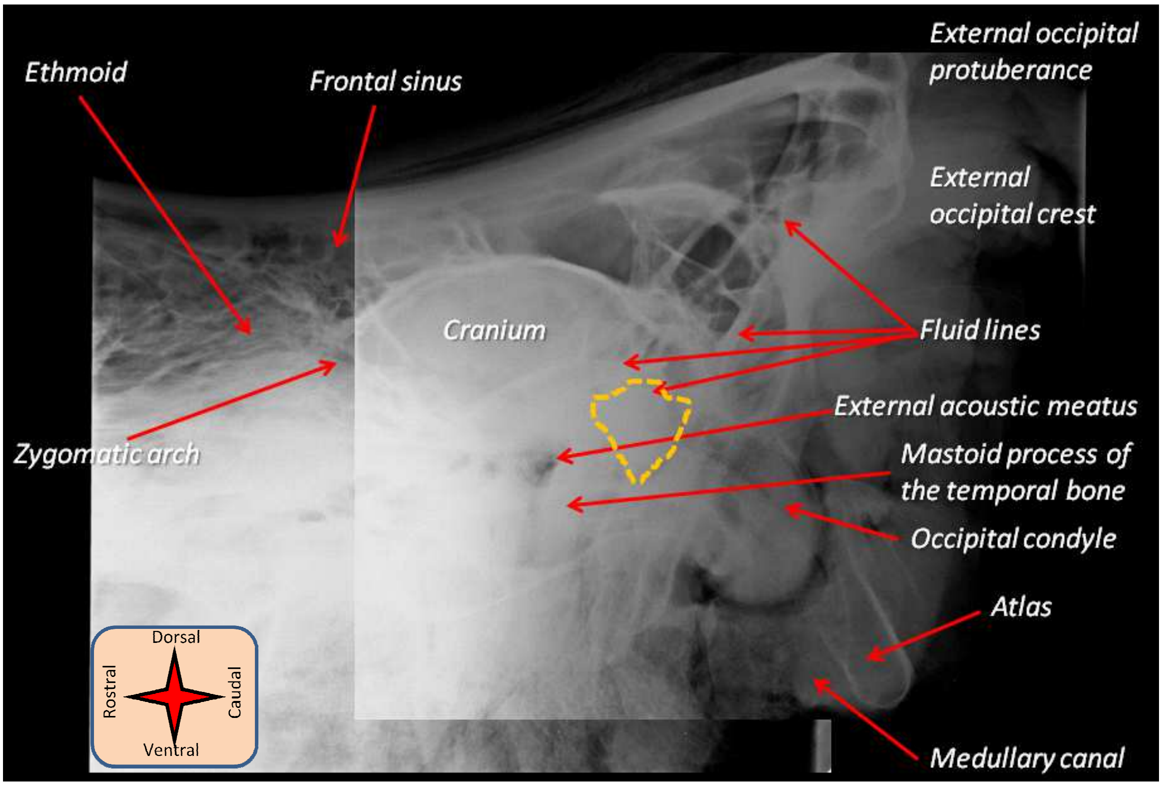

Figure 34: Lateral radiographic view of the caudal head of an adult southern white rhinoceros (Rhino 1). The orange dashed lines represent the position of the petrous part of the temporal bones.

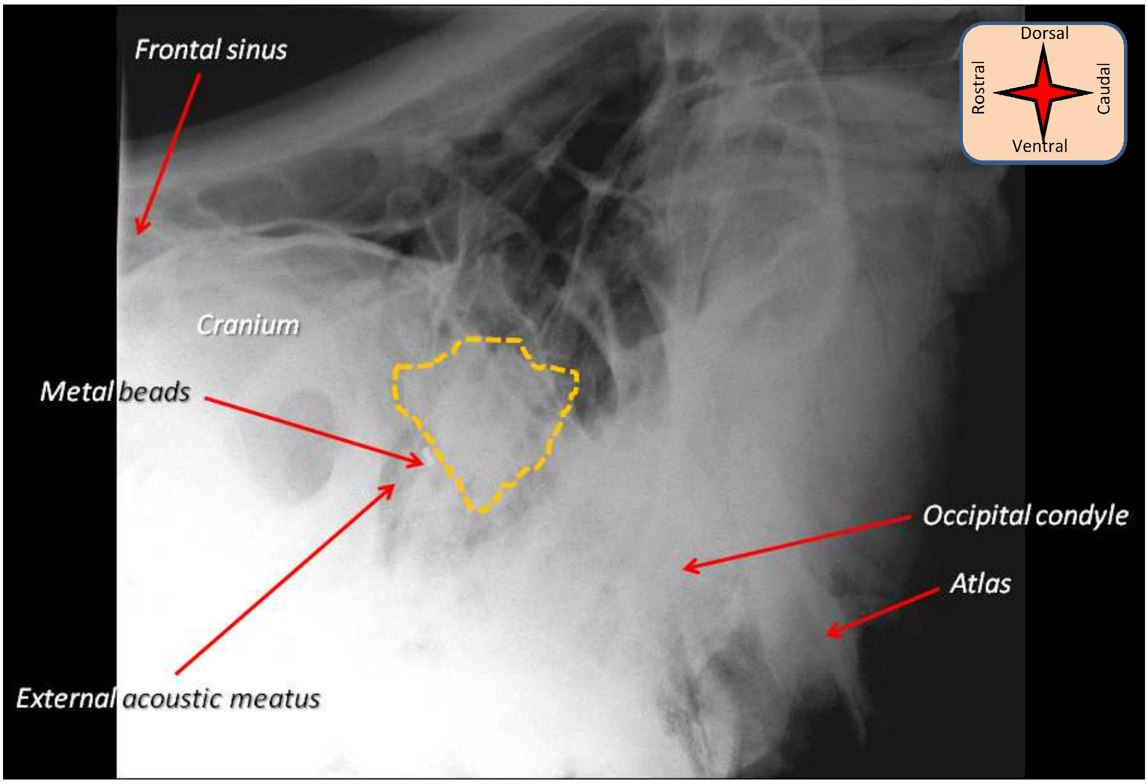

Figure 35: Left 30°Dorsal-Right Ventral Oblique (L30°D-RVO) radiographic view of the caudal head of an adult southern white rhinoceros (Rhino 1). A dog naso-gastric tube containing metal beads at its distal aspect was inserted all the way down the external ear canal. The orange dashed lines represent the position of the petrous part of the temporal bone on the side opposite to the X-ray generator.

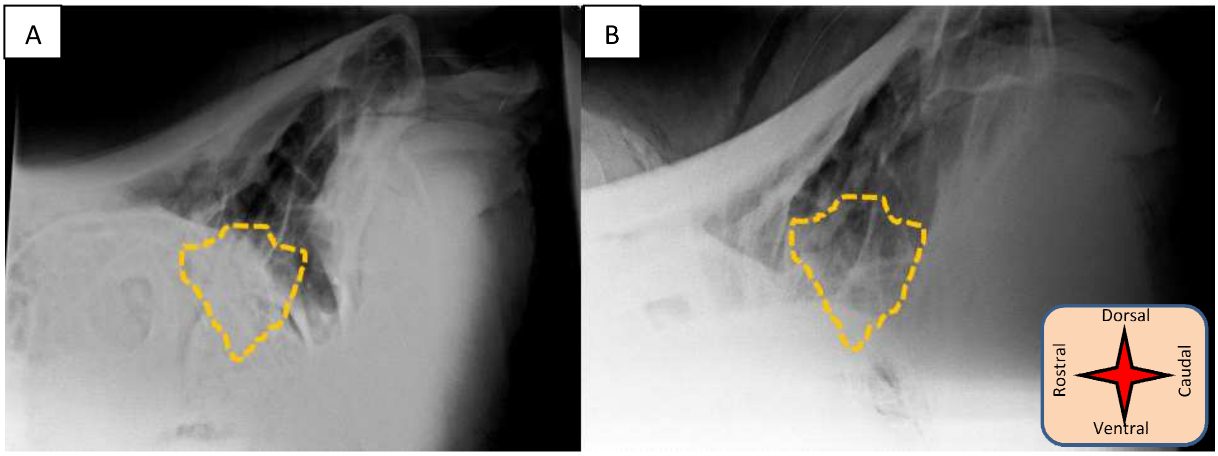

Figure 36: L45°D-RVO (A) and L60°D-RVO (B) radiographic views of the caudal head of an adult southern white rhinoceros (Rhino 1). The orange dashed lines represent the position of the petrous part of the temporal bone on the side opposite to the X-ray generator.

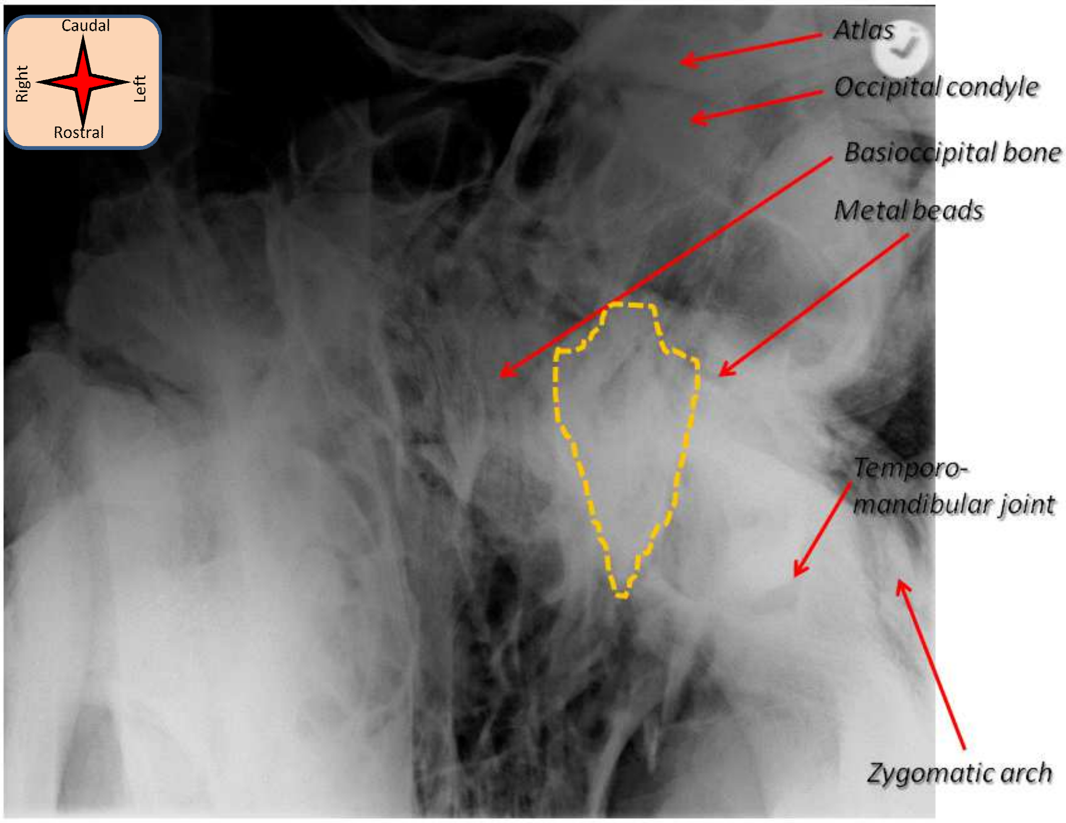

Figure 37: Dorso-ventral (slightly oblique) radiographic view of the caudal head of an adult southern white rhinoceros (Rhino 1). The orange dashed lines represent the position of the left petrous part of the temporal bone.

When looking at the radiographs obtained from the two neonates (Rhinos 3 and 4), a much better contrast and a better understanding of the regional anatomy could be obtained. All the bony structures of the caudal skull were clearly visible. Postmortem artifactual gas was present intracranially and within fascial planes (Figure 38 to 40).

On the LL view, the ear canal, the external acoustic meatus as well as the densely mineralised petrous part of the temporal bone with its internal acoustic meatus were nicely observed. The sutures lines between the basioccipital and basisphenoid bones, frontal and parietal bones, and lateral and squamous parts of the occipital bone were visible (Barone 2010a; Butler et al. 2017) (Figure 38). The 30°Dorsal to Ventral Oblique view allowed a better identification of the ear canal and petrous part of the temporal bone on the side contralateral to the generator. With the increasing obliquity of the 45°- and 60°Dorsal to Ventral Oblique views, the same structures were highlighted but increasing distortion and increasing loss of contrast were observed (Figure 39). On the DV view, the same image quality was obtained, especially on the smaller Rhino 3, allowing observation of the ear (Figure 40). Radiographic imaging of the pinna allowed the auricular cartilage and external ear canal to be visualised (Figure 41).

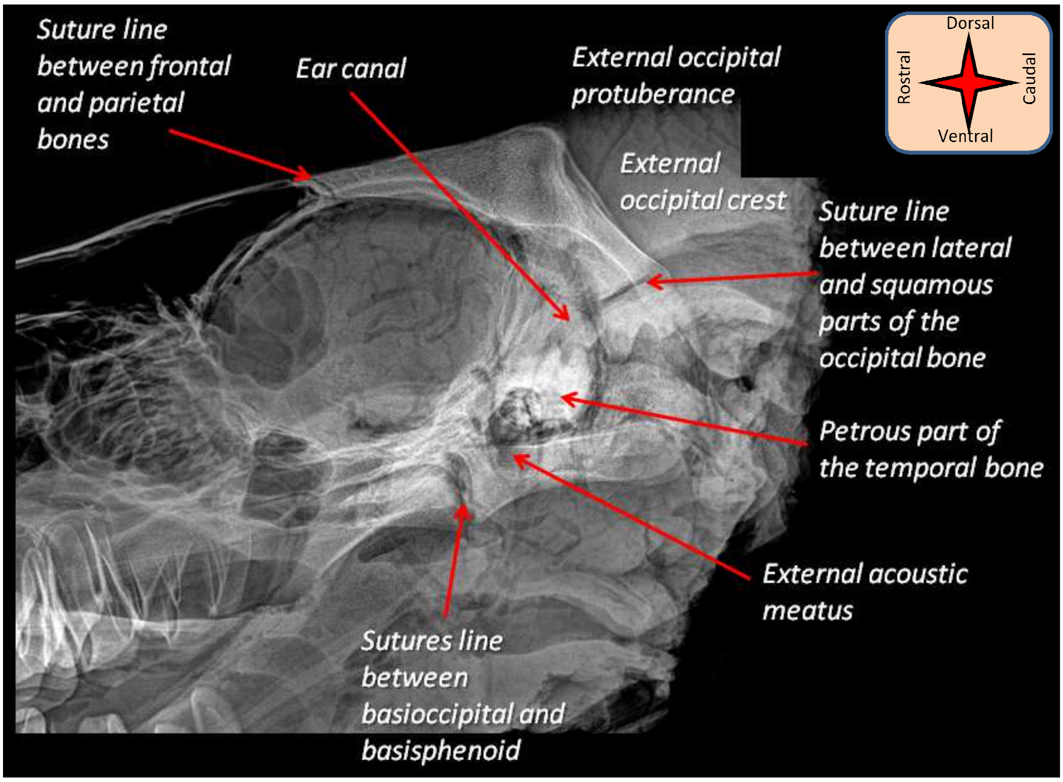

Figure 38: Lateral radiographic view of the caudal head of a neonate southern white rhinoceros (Rhino 3). Postmortem artifactual gas is visible intracranially and within fascial planes.

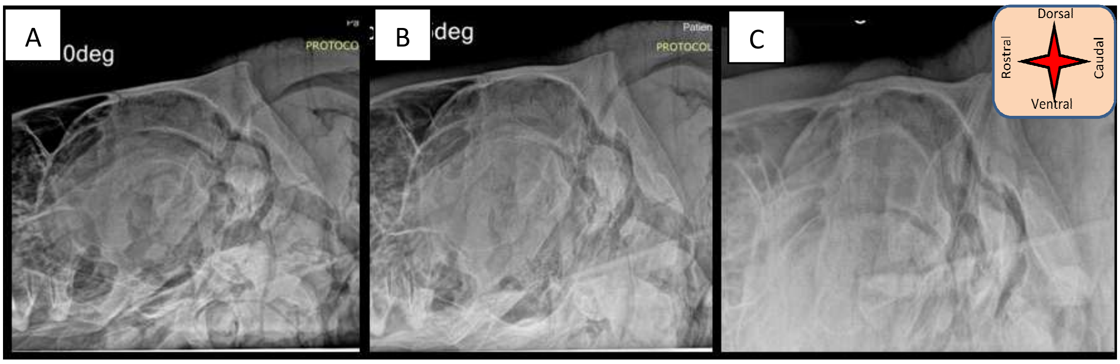

Figure 39: L30°D-RVO (A) , L45°D-RVO (B) and L60°D-RVO (C) oblique radiographic views of the caudal head of a neonate southern white rhinoceros (Rhino 3). Postmortem artifactual gas is visible intracranially and within fascial planes. Note the decreasing contrast and increasing distortion from A to C.

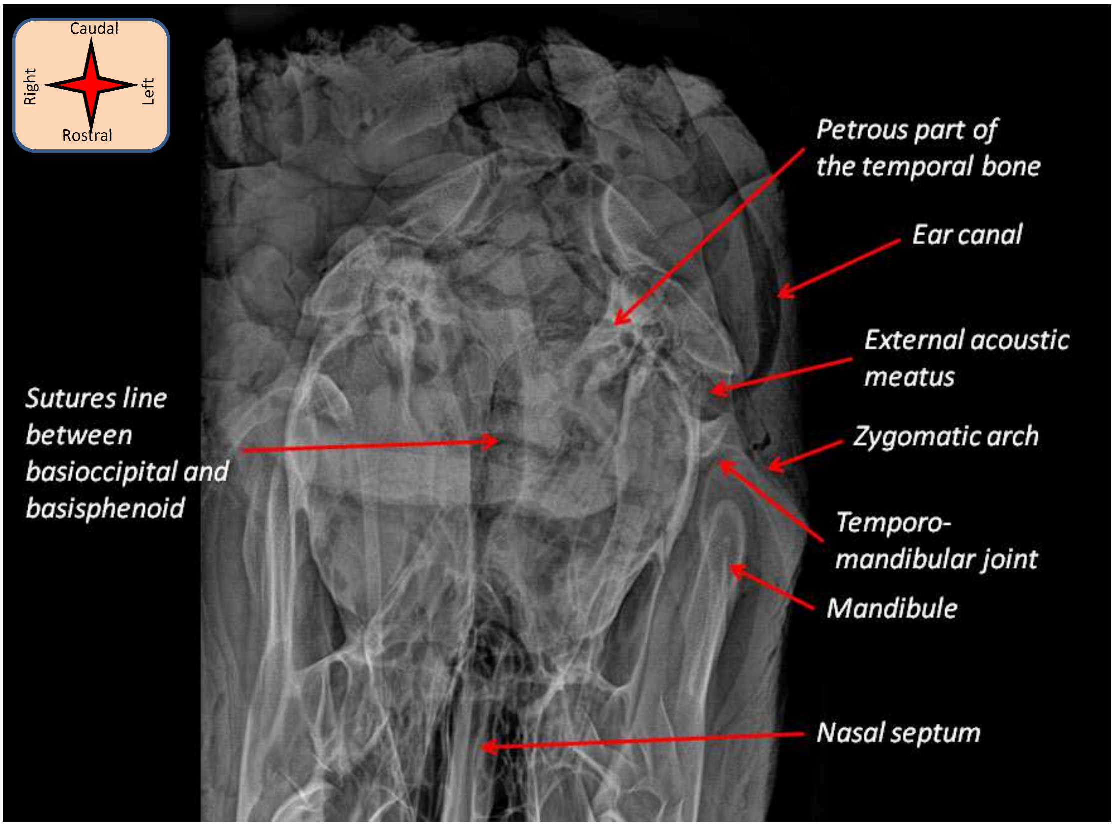

Figure 40: Dorso-ventral radiographic view of the caudal head of the caudal head of a neonate southern white rhinoceros (Rhino 3). Postmortem artifactual gas is visible intracranially and within fascial planes.

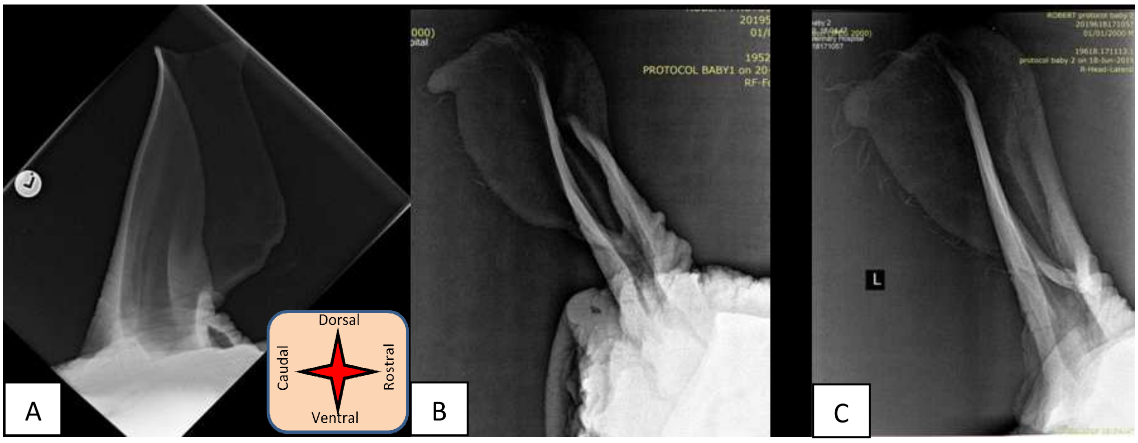

Figure 41: R45°D-LVO radiographic views focused on the pinna of Rhino 1 (A), 3 (B) and 4 (C). The shape of the auricular cartilage is visible.

4.5 Computed tomographic anatomy of the ear

The fresh heads of all four cases were CT-scanned. The neonate heads were scanned completely whereas only the caudal part of the head was acquired in Rhino 1 and 2 (Table 4).

Table 4: *CT equipment and parameters used in this study on four southern white rhinoceroses' heads.*

	Rhino 1	Rhino 2	Rhino 3		Rhino 4
CT scanner	Siemens Somatom Emotion Duo	Siemens Somatom Emotion Duo	Siemens Somatom Emotion Duo	Toshiba Aquilion 128 slice	Siemens Somatom Emotion Duo
kV	130	130	130	120	130
mAs	158	184	133	300	115
Slice thickness (mm)	3	3	2	0.5	2

Computed tomography allowed observation of the osseous and soft tissue structures of the ear in all the southern white rhinoceroses, regardless of their size, in different planes. Image quality was seen to decrease when the animals' size increased.

Measurements of the dense petrous part of the temporal bone, tympanic bulla, as well as skin thickness and external ear canal length and angle are depicted in Table 5. Beside the increase in size of both the petrous part of the temporal bone and the tympanic bulla with age, the incredible increase in skin thickness at the TMJ level, in line with the base of the pinna was also noticed.

When focusing on the temporal bone, all three parts were visible: squamous, tympanic and petrous. On all animals, the mastoid process, the internal acoustic meatus, the cochlea, the vestibule and the semi-circular canals were visible, from rostral to caudal respectively (Figure 42). The tympanic bulla was observed in all samples; in Rhino 4 it was filled with fluid. However, only low detail was obtained of the middle and inner ear regions, especially in the larger animals. The ossicle chain and the tympanic membrane were clearly distinguishable only on the 128-slice CT of rhino 3 (Figure 43 and 44). When looking at the dual-slice CT of Rhino 3 (Figure 44) these structures were blurry compared to the 128-slice CT images. It is likely from the higher slice thickness used on the former examination but also from the lower resolution of the dual-slice CT.

Table 5: *CT measurements on four southern white rhinoceroses' heads.*

	Rhino 1		Rhino 2		Rhino 3		Rhino 4	
Skin thickness at temporo-mandibular joint level (mm)								
	21		12		7.7		8.6	
	Left	Right	Left	Right	Left	Right	Left	Right
Tympanic bulla								
Length (mm)	27.8	26.8	23.9	25.5	20.7	21.3	Fluid filled	Fluid filled
Height (mm)	28.3	26.6	20.4	18.7	8.3	11.5	Fluid filled	Fluid filled
Width (mm)	13.8	12.5	9.3	9.3	6.4	6.5	Fluid filled	Fluid filled
Petrous part of temporal bone								
Length (mm)	34.3	32.7	27.2	27.9	27.3	26.1	30.4	28.4
Height (mm)	44.6	46.8	31.1	28.4	20.8	22.1	26.1	25.9
Width (mm)	23.1	22.4	23.1	24.1	17.6	18.9	17.3	17.6
Horizontal ear canal								
Length (cm)	7.67	missing	5.06	5.03	3.63	2.69	3.61	3.80
Angle of horizontal ear canal from sagittal plan (degrees)	62	68	68	64	64	64	74	79

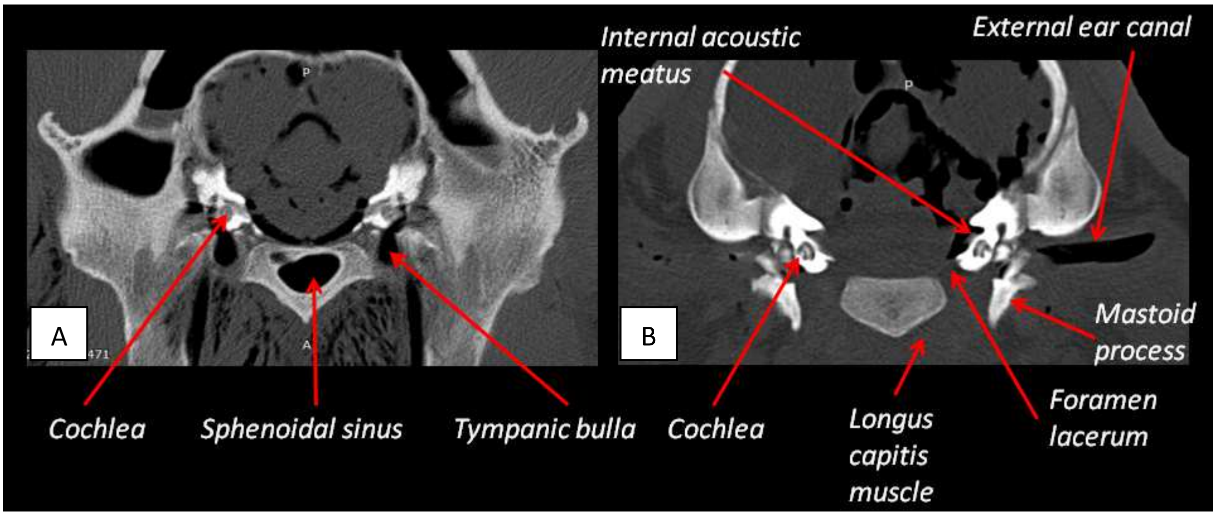

Figure 42: Transverse CT images at the level of the petrous part of the temporal bone obtained with a dual-slice CT in Rhino 1 (A) and 4 (B). 2mm slice thickness in A; 3mm slice thickness in B; Window width 1500 HU; Window level 450 HU. HU: Hounsfield units.

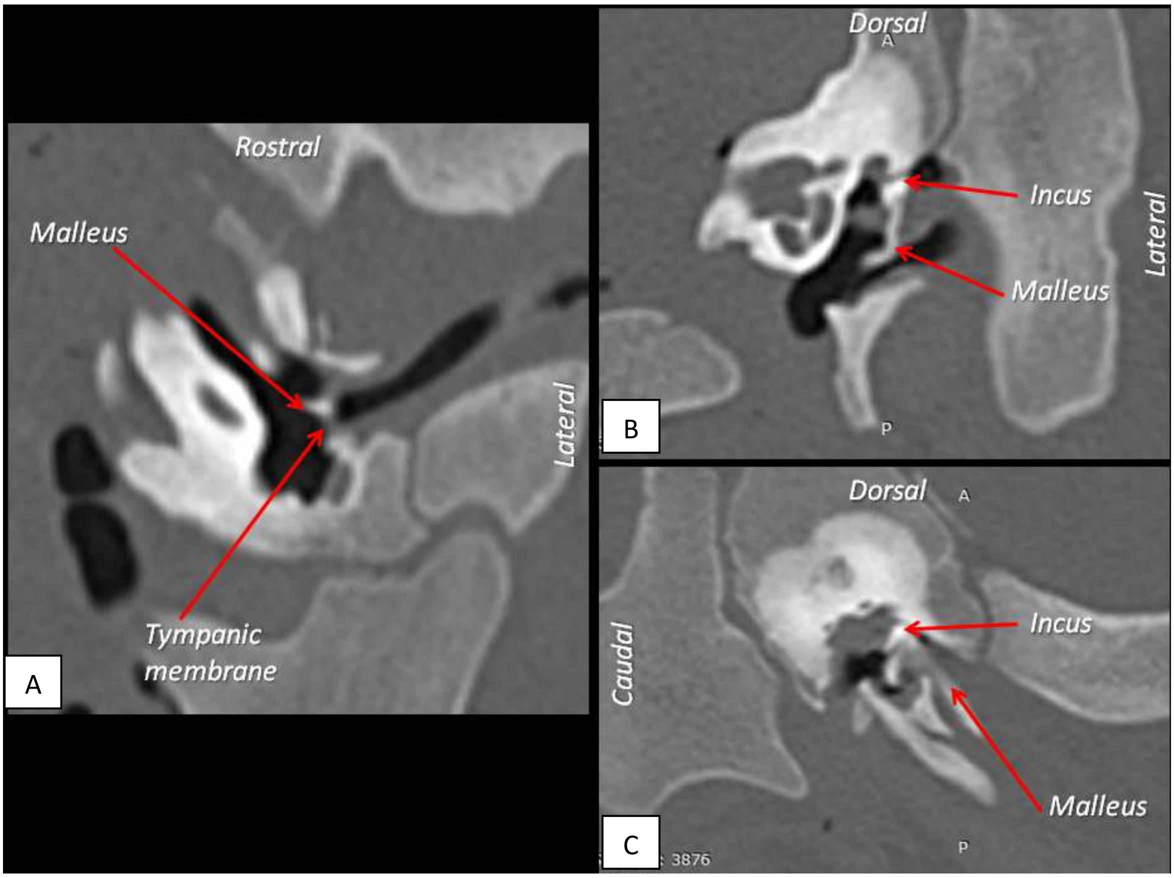

Figure 43: Coronal (A), transverse (B) and parasagittal (C) views of the middle and inner ear obtained from the left ear of Rhino 3 using a 128-slice CT. 0.5mm slice thickness in B; Window width 2700 HU; Window level 350 HU. HU: Hounsfield units.

Figure 44: Coronal CT images at the level of the left petrous part of the temporal bone of Rhino 3 obtained with a dual-slice CT (A) and a 128-slice CT (B). The ossicle chain is only visible on B (red arrow). A appears very blurry in comparison to B. Slice thickness: 2mm in A, 0.5mm in B; Window width: 1500 HU in A, 2700 HU in B; Window level: 450 HU in A, 350 HU in B. HU: Hounsfield units.

Finally, CT allowed 3D reconstruction of the southern white rhinoceros' heads to be done. Doing so, details on the osteology of this region could be obtained. The visible suture lines in the neonates made identification of each bone very easy. For instance, the temporal bone articulations with the mandible ventrally, parietal bone dorsally, occipital bone caudally, zygomatic bone rostrally and the sphenoid bone medially were clearly visible (Figures 45 to 48).

The development of the caudal skull with age was also observed when comparing 3D reconstructions of the four animals. In particular, the increasing size of the external occipital protuberance with age was visible (Figure 49).

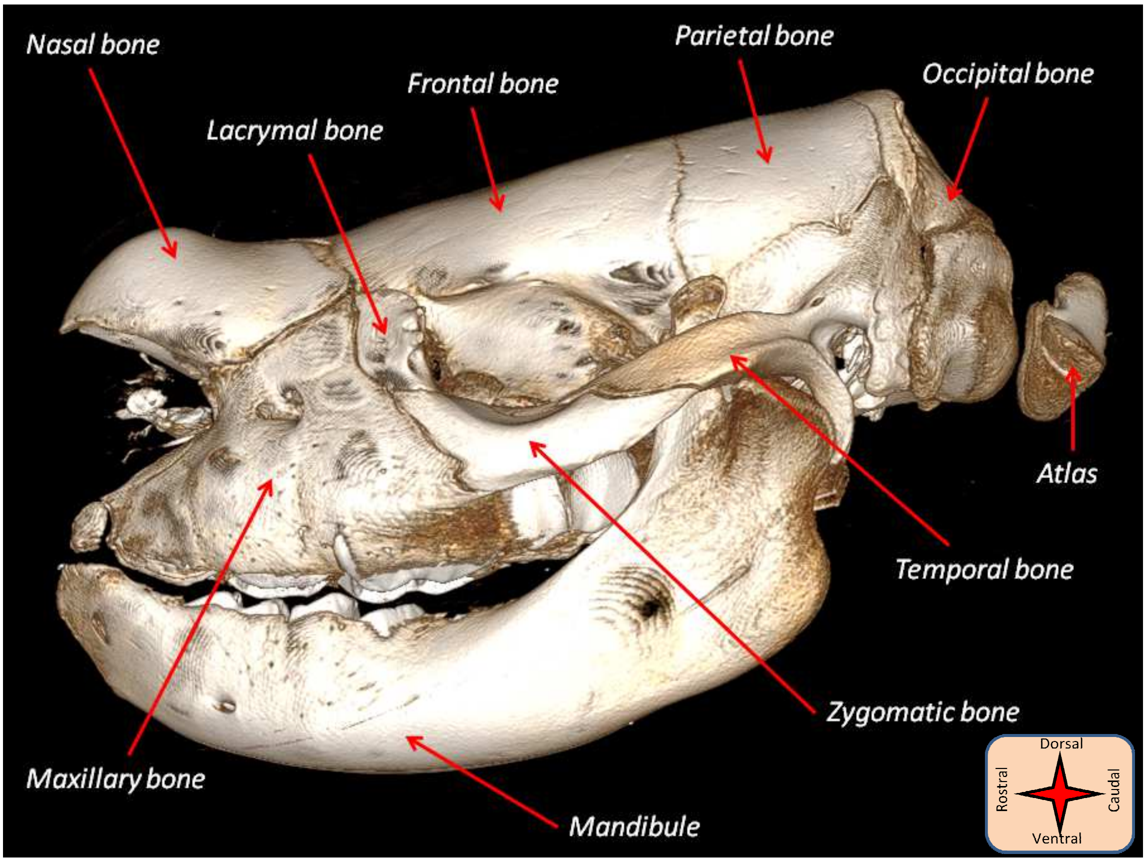

Figure 45: 3D reconstruction of the full skull of Rhino 3 using a 128-slice CT. Lateral view. The bones are named.

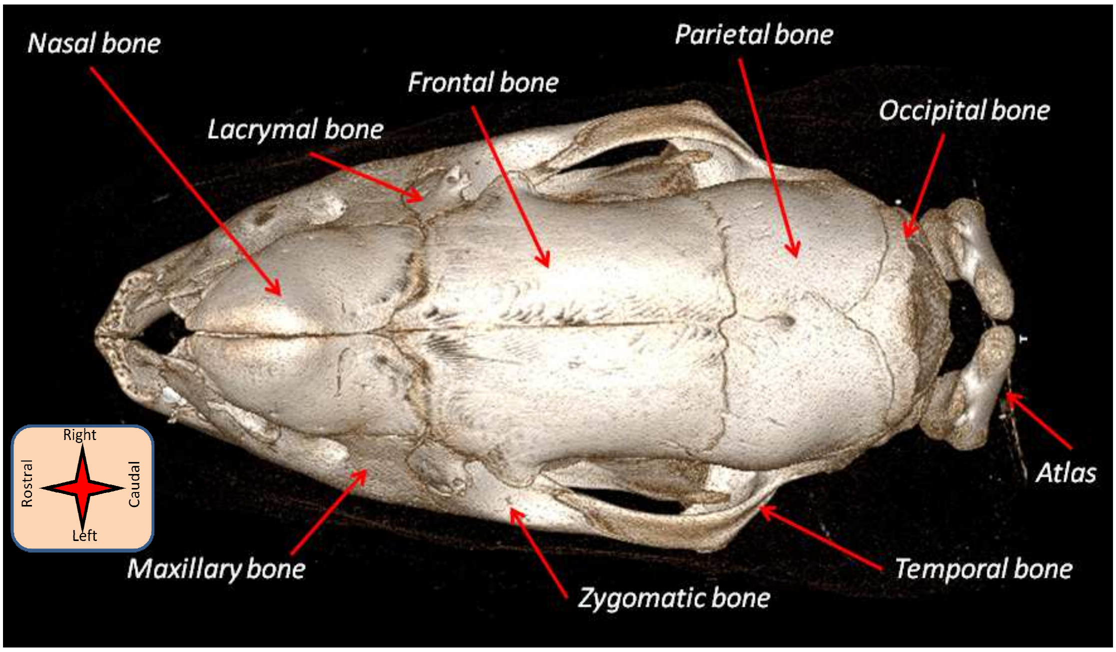

Figure 46: 3D reconstruction of the full skull of Rhino 3 using a dual-slice CT. Dorsal view. The bones are named.

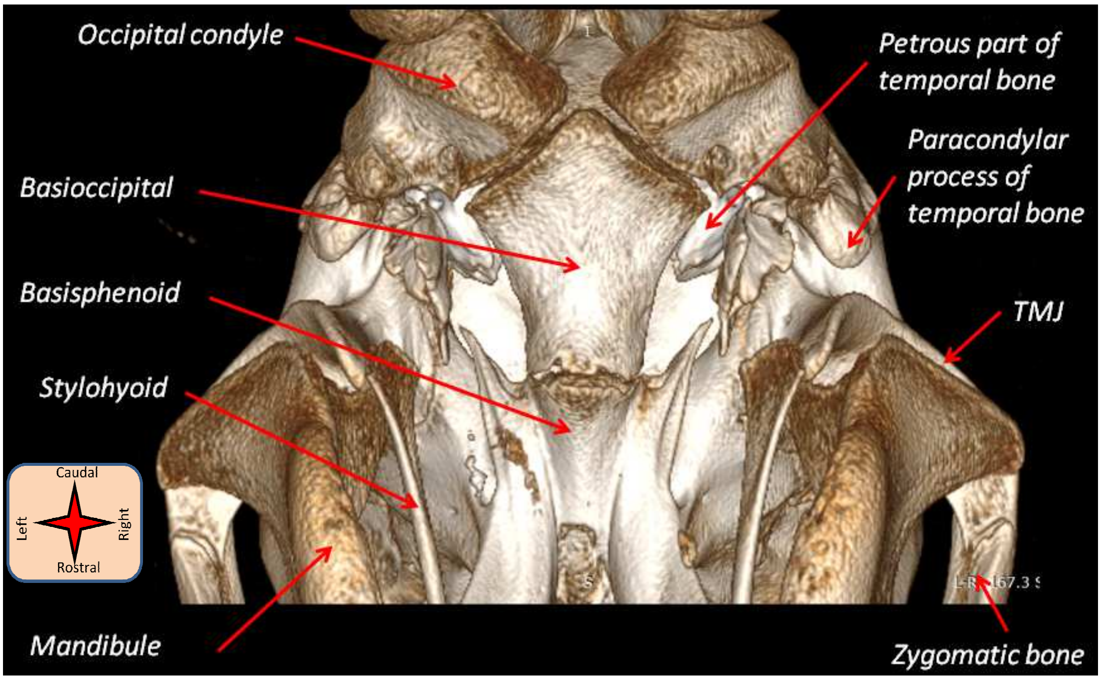

Figure 47: 3D reconstruction of the caudal skull of Rhino 3 using a 128-slice CT. Ventral view. The bones are named.

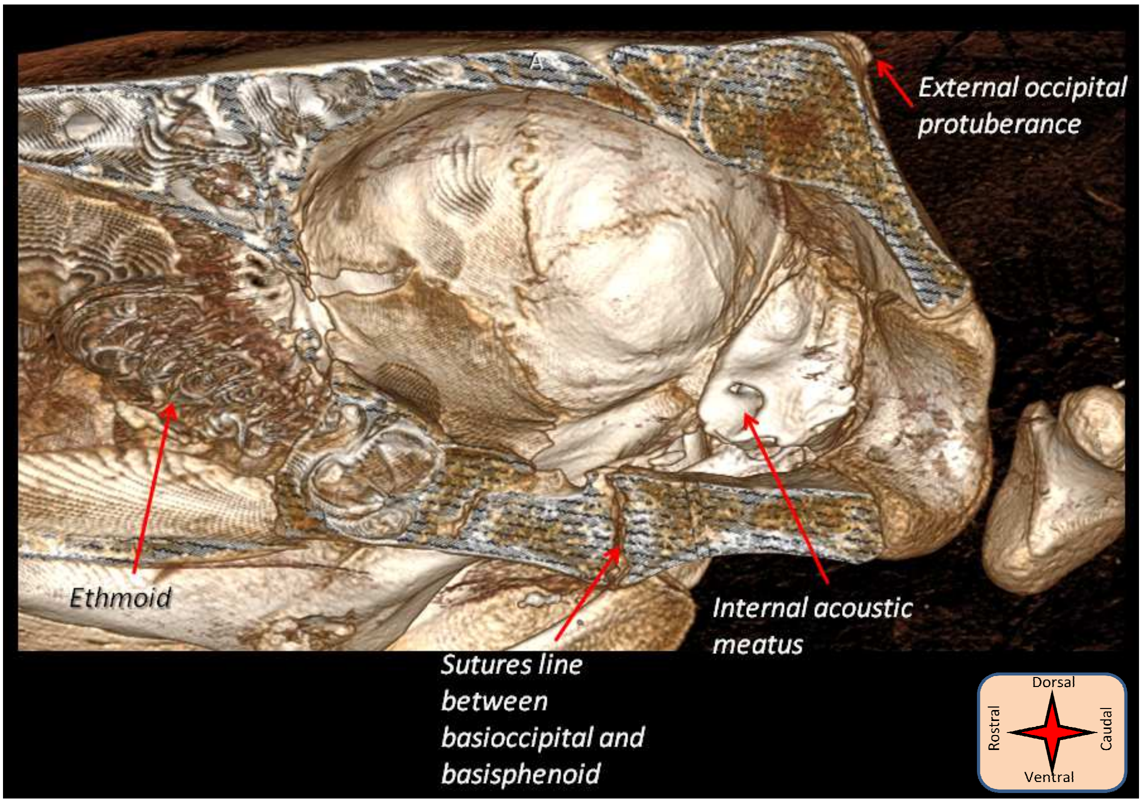

Figure 48: 3D reconstruction of the caudal skull of Rhino 3 using a 128-slice CT. Right medial view. Some bones are named.

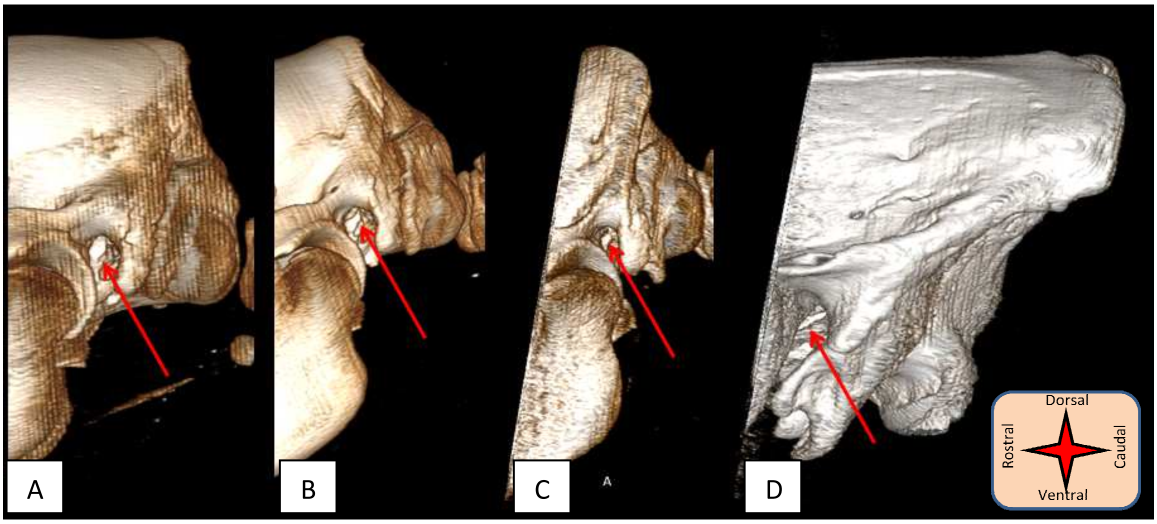

Figure 49: 3D reconstruction of the caudal skull of Rhino 4 (A), 3 (B), 2 (C) and 1 (D) using a dual-slice CT. Lateral view. The red arrow points to the external acoustic meatus.

4.6 Micro-anatomy of the ear

Excellent image quality was obtained for all samples, with a mean voxel size of 39,5 +/- 6,4 µm (Table 6). Scanning time was 66.8 minutes for each sample.

The tympanic membrane, middle ear and inner ear structures were visible in all samples (Figures 50 and 51).

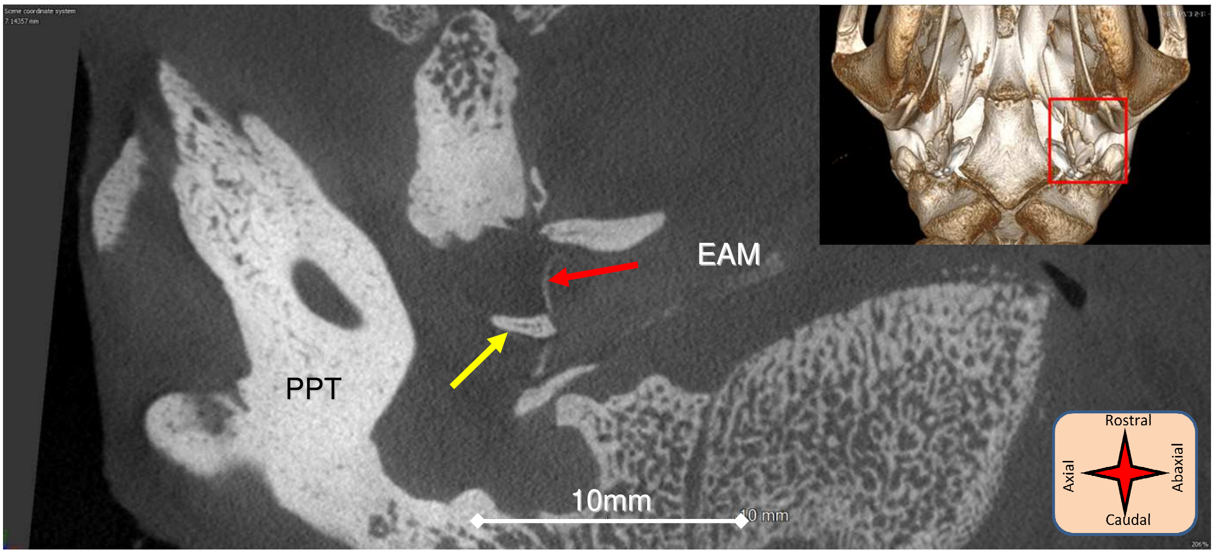

Figure 50: Micro-CT image obtained from the left ear of Rhino 3, coronal plane. The red arrow shows the tympanic membrane. The yellow arrow highlights the handle of the hammer (*manubrium malleus*) attached to the tympanic membrane. PPTB: Petrous part of the temporal bone. EAM: External acoustic meatus. Scale is 10mm. The top right insert shows the region that has been scanned with the micro-CT; this ventral view of Rhino 3 was obtained with a 128 slice CT scan.

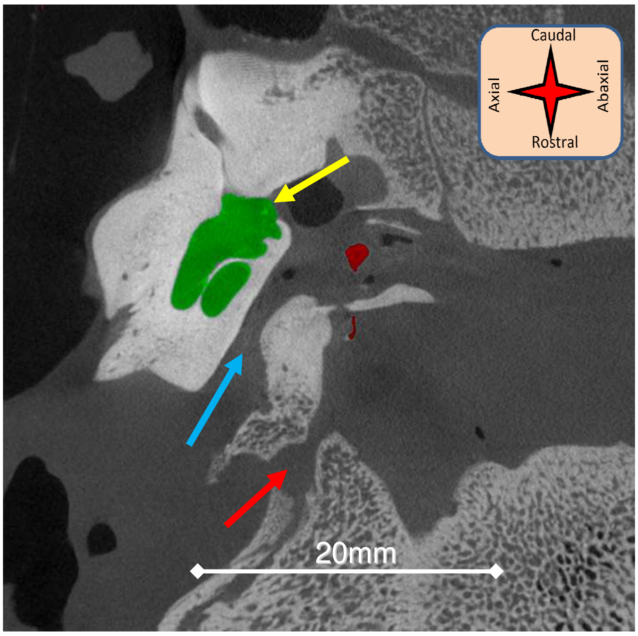

Figure 51: Micro-CT image obtained from the right ear of Rhino 4, coronal plane. The green area shows the cochlea. The red areas highlight the handle and the rostral branch of the hammer (*malleus*). The blue arrow indicates the auditory tube. The red arrow indicates the path of the internal carotid artery. The yellow arrow shows the round window (*fenestra cochleae*). Scale is 20mm.

Volumes of the middle ear ossicles and inner ear structures (semi-circular canals, vestibule and cochlea) are reported in Table 6.

Table 6: *Voxel size, inner ear volume and middle ear ossicles volume measured using micro-CT images in the left and right ear of two southern white rhinoceroses.*

		Voxel size (µm)	Inner ear volume (mm^3)	Middle ear ossicles volume (mm^3)
Rhino 3	Left ear	34,1	240,65	28,82
	Right Ear	35,8	189,71	31,41
Rhino 4	Left ear	39,8	234,88	34,11
	Right Ear	48,4	232,4	37,55
	Mean	39,5	224,41	32,97
	Standard Deviation	6,4	23,39	3,74

Tridimensional reconstructions of the middle ear ossicles and inner ear structures were of high quality (Figures 52 to 61).

The hammer (*malleus*) has a Y-shaped configuration. The rostral branch of the Y appears straight, lateral ventrally, longer than the handle of the hammer, facing rostral. The handle of the hammer lies more sagittally ventrally, is curved (ventro-medial to dorso-lateral), points down, and attaches to the tympanic membrane. The base of the Y-shaped *malleus* is the head of the hammer. It is dorsal to the handle and the rostral branch and articulates caudally with the body of the *incus* through the incudomalleolar joint which is clearly visible on our images (Figures 52 and 53).

The *incus* has more of a ladle shape. The cup of the ladle is the body of the *incus*, is wider and articulates with the head of the *malleus* rostrally. The handle of the ladle, or long crus (or process) of the *incus*, then curves caudo-medially, forming the lenticular process of the *incus*, articulating with the head of the stirrup (*stapes*) through the incudostapedial joint. Dorsally the cup part of the ladle (body of the *incus*) sends a lateral pointy projection, the short crus of the *incus* (Figures 52 and 54).

The *stapes* was clearly visible, smaller than the other two ossicles. Its head articulates with the long process of the *incus*, whereas its base or footplate is attached to the membrane, or annular ligament, of the oval window (*fenestra ovalis*) on the vestibule (Figures 52, 54 and 55). Because of the fixative fluid contained in the middle ear, no soft tissue structures could be identified.

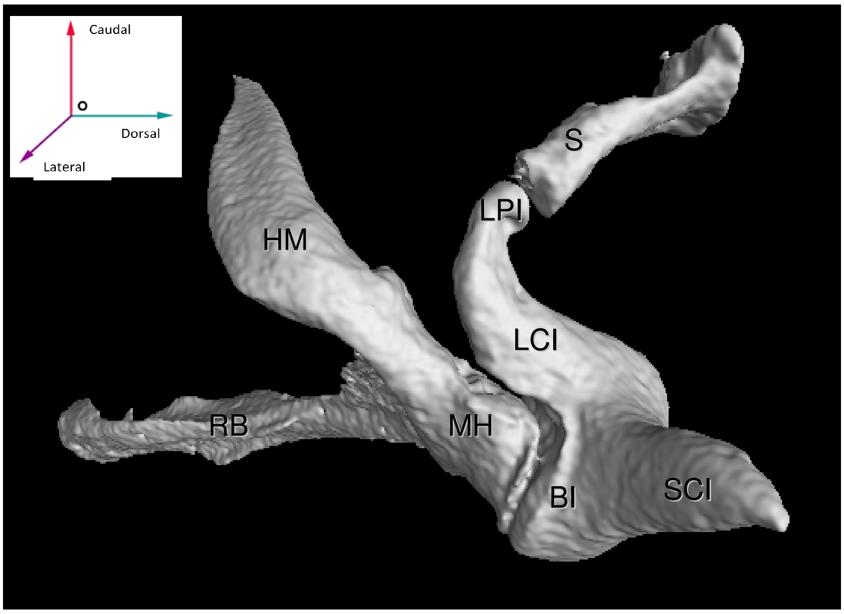

Figure 52: 3D reconstruction of the auditory ossicles obtained from the left ear of Rhino 3. The body of the *incus* (BI), short crus of the *incus* (SCI), long crus of the *incus* (LCI), lenticular process of the *incus* (LPI), *malleus* head (MH), handle of the *malleus* (HM), rostral branch of the *malleus* (RBM) and *stapes* (S) are all visible.

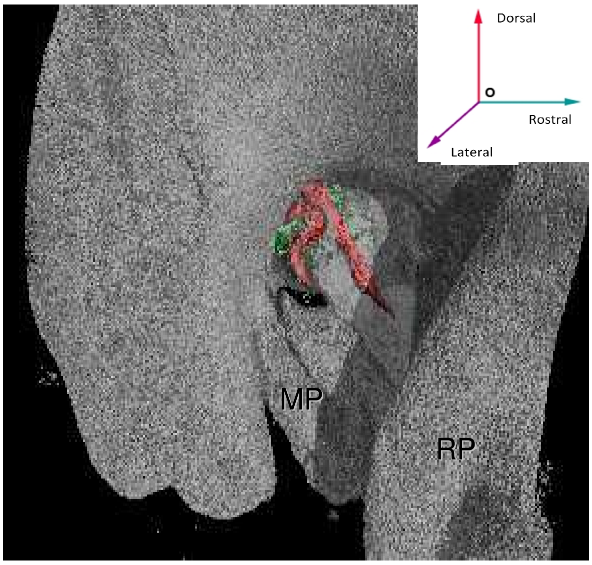

Figure 53: 3D reconstruction of the external acoustic meatus with auditory ossicles (red) and inner ear (green) in place, obtained from the left ear of Rhino 4. Lateral view. The two branches of the *malleus* are clearly visible. MP: Mastoid process of the temporal bone; RP: Retroarticular process (according to Endo et al. (1998))

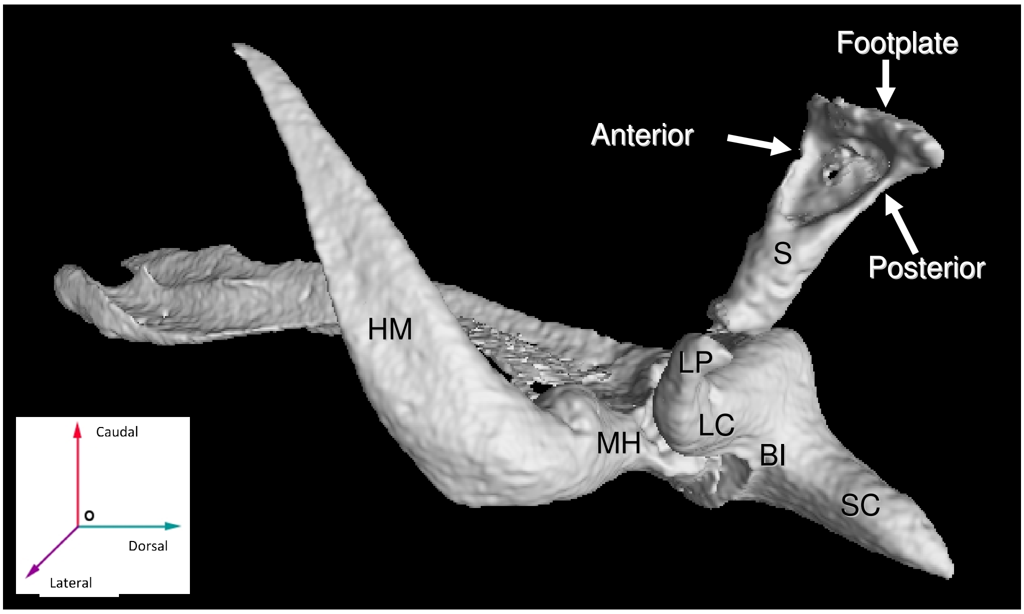

Figure 54: 3D reconstruction of the auditory ossicles obtained from the left ear of Rhino 3. The body of the *incus* (BI), short crus of the *incus* (SCI), long crus of the *incus* (LCI), lenticular process of the *incus* (LPI), *malleus* head (MH), handle of the *malleus* (HM) and *stapes* (S) with his anterior and posterior crus, as well as footplate, are all visible.

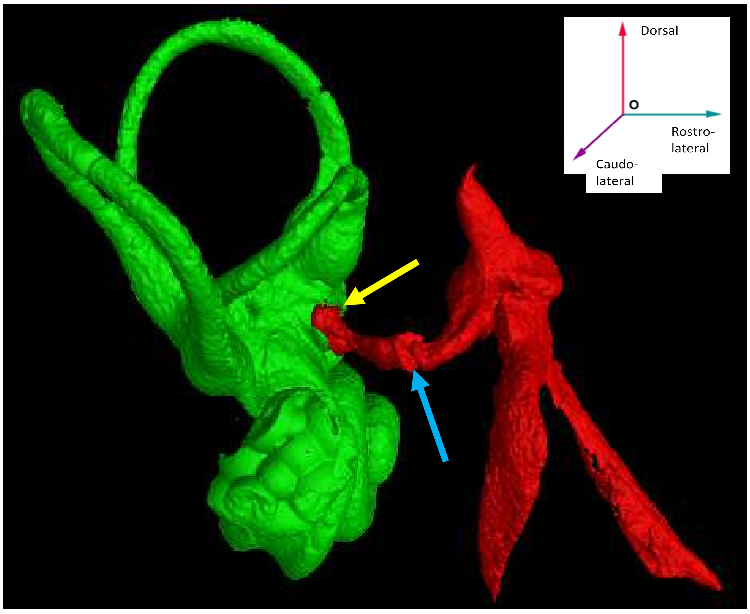

Figure 55: 3D reconstruction of the auditory ossicles (red) and osseous labyrinth (green) obtained from the left ear of Rhino 4. Lateral view. The attachment of the base of the *stapes* to the *fenestra ovalis* (yellow arrow) as well as the incudostapedial joint (blue arrow) are clearly visible.

When looking at the bony structures of the inner ear, or osseous labyrinth, the cochlea appears as a spiral channel starting at the vestibule and describing 2 turns rostro-laterally around its axis, with an medial direction of rotation (Figures 56, 57 and 58). The tympanic and vestibular ducts with associated septa (the osseous spiral lamina) are visible in the cochlea, as well as the central *modiolus*. The cochlear aqueduct is also visible running from the basal cochlear turn to the *posterior cranial fossa* (Figure 57). Similarly the vestibular aqueduct between the vestibule and the *posterior cranial fossa* is also observed.

All 3 semicircular canals emerge from the caudo-dorsal part of the vestibule (Figures 56, 59, 60 and 61). The anterior and the posterior canals have a common part, or common crus, medially, whereas the lateral one is clearly isolated. The *ampullae* of the canals, one anterior, one posterior and one lateral are also visible.

In the vestibule, even though some septae are sometimes visible, it is not possible to visualize the utricle and saccule.

From human studies, the position of the nerves (facial and vestibulocochlear) and vessels (internal carotid artery, sigmoid sinus and internal jugular vein) associated to the middle and inner ears could also be assumed (Figures 58 and 61) (Moon & Lee 2014; Nayak 2001; Qiu et al. 2003).

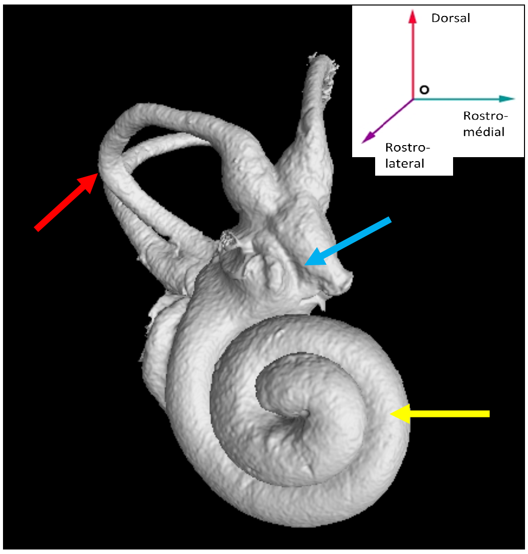

Figure 56: 3D reconstruction of the bony structures of the inner ear, obtained from the left ear of Rhino 3. Rostro-lateral view. The yellow arrow highlights the 2 turns of the spiral cochlea. The blue arrow points to the vestibule. The red arrow points to the semicircular canals.

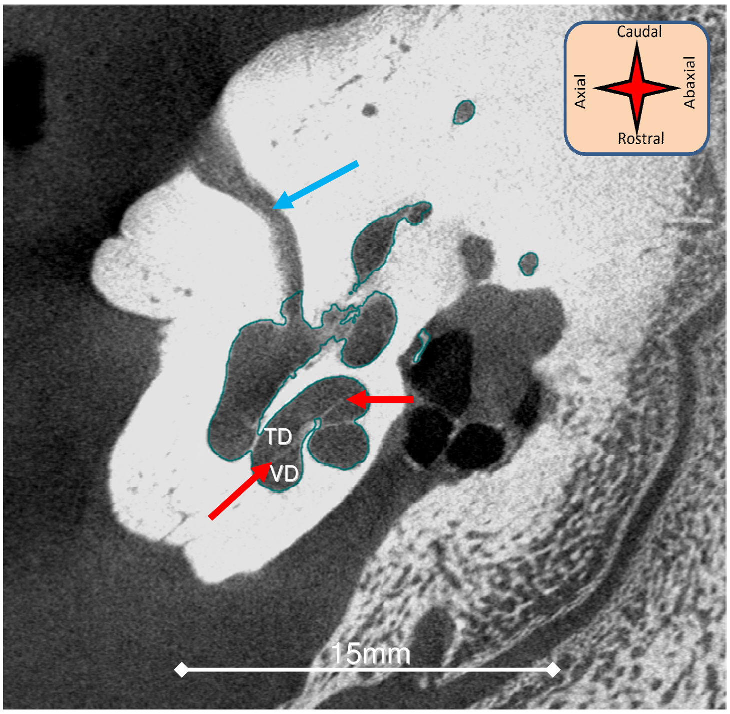

Figure 57: Micro-CT image obtained from the left ear of Rhino 4, coronal plane. The tympanic (TD) and vestibular (VD) ducts with associated osseous spiral lamina (red arrows) are visible in the cochlea. The cochlear aqueduct is also clearly visible (blue arrow).

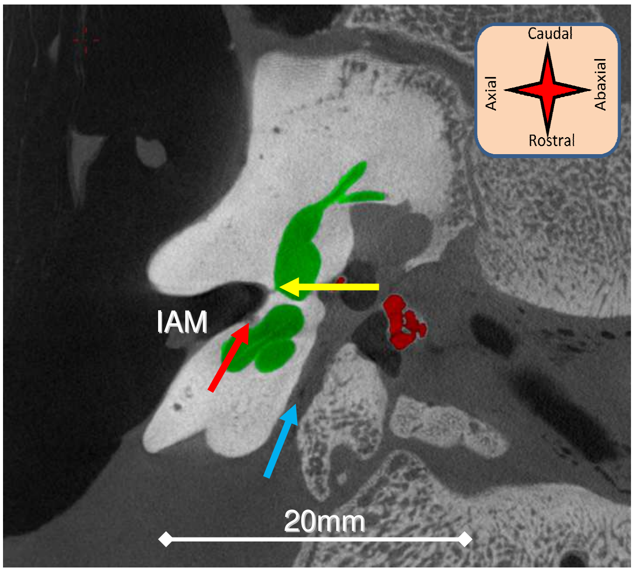

Figure 58: Micro-CT image obtained from the right ear of Rhino 4, coronal plane. The green area shows the cochlea. The red areas highlight the *stapes* and the incudomalleolar joint. The facial canal (blue arrow) and tracts of the cochlear (red arrow) and vestibular (yellow arrow) nerves are visible. IAM: Internal acoustic meatus.

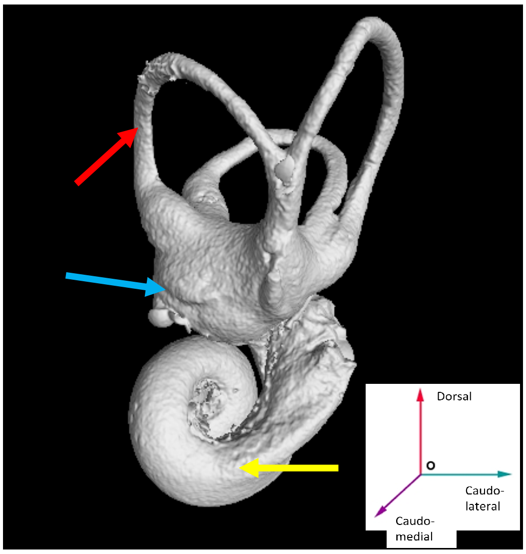

Figure 59: 3D reconstruction of the bony structures of the inner ear, obtained from the left ear of Rhino 3. Caudo-medial view. The yellow arrow highlights the 2 turns of the spiral cochlea. The blue arrow points to the vestibule. The red arrow points to the semicircular canals.

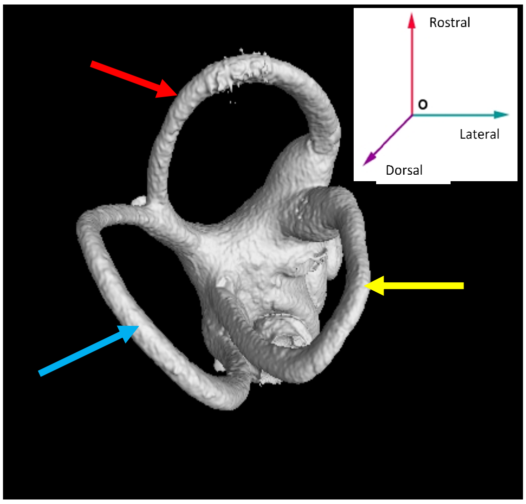

Figure 60: 3D reconstruction of the bony structures of the inner ear, obtained from the left ear of Rhino 3. Dorsal view. The yellow arrow highlights the lateral semicircular canal. The blue arrow points to the posterior semicircular canal. The red arrow points to the anterior semicircular canal.

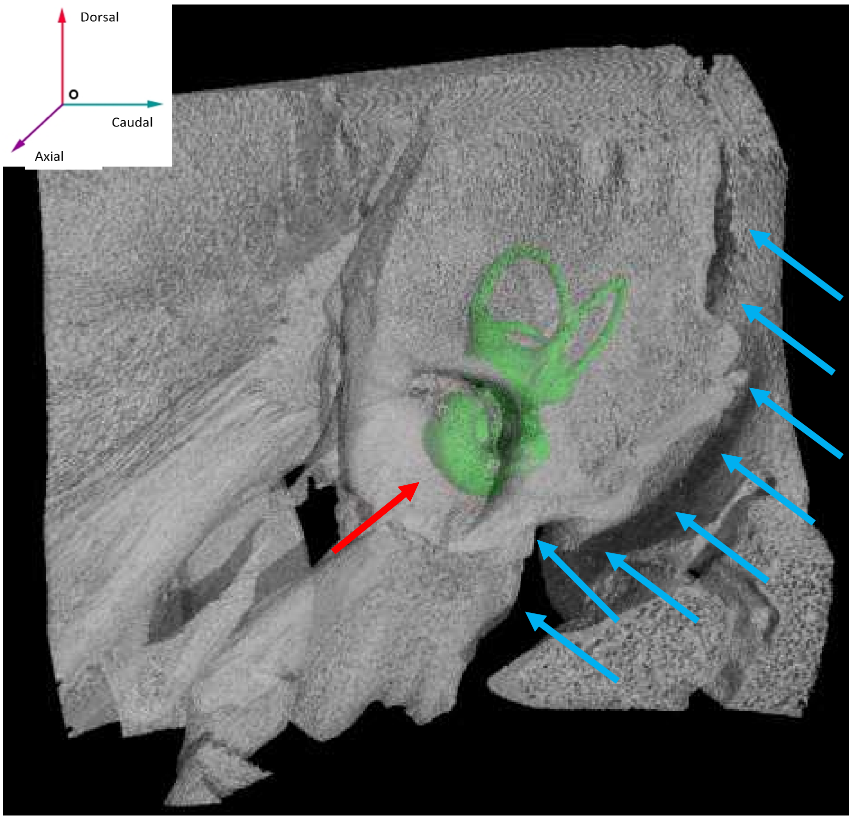

Figure 61: 3D reconstruction of the inner ear (green) obtained from the left ear of Rhino 3. Medial view. The orientation of the cochlea and semicircular canals relative to the internal acoustic meatus (red arrow) through which runs the vestibulocochlear and facial nerves is shown. The tract of the sigmoid sinus and internal jugular vein is highlighted by the blue arrows (according to Qiu et al. (2003)).

CHAPTER 5: DISCUSSION

5.1 Anatomical dissection of the ear

Dissection of the ear in the southern white rhinoceros showed many similarities with that of another Perissodactyle, namely the horse.

Isolating and identifying the different muscles proved to be difficult with the available literature. For instance, the early description from Saban (1970) appeared very simplistic and inaccurate. Compared to the horse (Barone 2010b), some muscles had different proportions, or even appeared not to be present in the rhinoceros. Among them, the *m. zygomaticoauricularis* was not observed in our samples. Hence, it could be simply absent in the rhinoceros, might be present only as an aponeurotic or fibrous band between the zygomatic arch and the auricular cartilage, as described on Figure 8, or less likely present as a very thin muscle band adherent to the skin that was removed with the latter. Alternatively, it could have fused with other muscles performing similar functions.

The interscutularis muscle appeared as a transverse continuous band in the southern white rhinoceros. In the horse, a median raphe is described, with an insertion on the external sagittal crest reaching the temporal line. Those were not observed in this study.

Similarly, different anatomy between the cranium of the horse and that of the rhinoceros leads to different insertional patterns. As an example, the zygomaticoscutularis muscle cannot reach the zygomatic arch in the rhinoceros because this species does not have a zygomatic process of the frontal bone. Instead it reaches the orbital ligament and the frontal bone.

Unfortunately, the neurovascular supply to the ear muscles was not clearly visible most of the time. It is likely due to post-mortem autolysis that occurred before the heads were put into formalin.

Variations in the branches of the external carotid artery between mammal species is well described (Barone 2011). It appears from our dissection that the blood supply of the ear in the southern white rhinoceros is different from what has been described for the horse (Barone 2011). In particular, the caudal auricular artery emerges from the external carotid artery way before the linguofacial trunk and the deep auricular artery appears to emerge from the maxillary artery. This latter point is similar to humans. The *stylomastoidea* artery rising from the deep auricular artery in the horse has not been visualized. It could then possibly emerge from the occipital artery in the rhinoceros, as described in the bovine. The different auricular rami (lateral, medial and intermediate) reported in other species were not clearly observed in our samples. It is interesting to note that the transverse facial artery was not visualized either. Further investigations using latex casts and angiographic studies would provide further information to perfectly describe the blood supply of the ear in the southern white rhinoceros (Khairuddin et al. 2015).

The caudal auricular vein, and especially its branch running towards the apex of the pinna was clearly visible under the thin skin. It is easily accessible and explains why it has been used clinically for injections and catheter placement (Miller & Buss 2014; Zeiler & Stegmann 2012).

Whereas the facial nerve itself was visible on our samples, its small branches innervating the external ear could not be observed. It is assumed that they run between the auricular muscles and under the parotid gland to give the auriculo-palpebral nerve rostrally and the caudal auricular nerve caudally, similar to what happens in horses (Barone 2011). This will have to be confirmed in future studies.

When looking at the auditory tube of the southern white rhinoceros, differences were visible from its equine counterpart. As previously described, no guttural pouch was present in our neonate southern white rhinoceroses and the auditory tube consists of a simple canal with cartilage wall (Endo et al. 1998; Endo et al. 2009). In the horse, the *plica salpingopharyngea* is a mucosal fold on the floor of the tubular entryway into the auditory tube, attached medially to a cartilaginous flap and laterally to the lateral wall of the pharynx (Freeman & Hardy 2012). In the rhinoceros, the pharyngeal opening of the auditory tube appeared as a large opening without cartilaginous or mucosal coverage. In the adult white rhinoceros, a length of 145mm and diameter of 7mm have been reported for the auditory tube (Endo et al. 1998). Our smaller measurements correlate with the size of our neonate heads.

In man, the cartilage of the Eustachian tube is reportedly of a similar composition and elasticity to the one of the pinna (Nayak 2001). In the southern white rhinoceros, the wall of the auditory tube is composed of hyaline cartilage mainly (Endo et al. 1998) but no comparison was made with the composition of the pinna.

5.2 Radiographic anatomy of the ear

The same pitfalls as described in equine radiology apply to the southern white rhinoceros (Butler et al. 2017). It appeared that radiographic evaluation of the ear region of the southern white rhinoceros was possible but much easier in smaller animals than in adults. In the latter, thickness of the head and superimposition of structures made acquisition and interpretation of the radiographs respectively very tedious, despite using much higher parameters than in horses (Butler et al. 2017).

Another factor to consider is the fact we only used Computed Radiography on the adult rhinoceros and it is possible that better contrast would have been obtained with the Digital Radiography equipment we used on the neonates. Unfortunately the DR was not available at that time.

Portable machines used in the field are unlikely to provide adequate penetration in the rhinoceros, especially in adult animals with very large heads and very thick skin. Additionally, even in horses that have smaller heads, diagnosing affections of the middle ear, temporohyoid joint or inner ear is difficult with radiographs only (Divers et al. 2006; Pownder et al. 2010; Slovis 2012; Walker et al. 2002). It is likely to be even more complicated in the southern white rhinoceros. Thus we believe the diagnostic value of this modality to detect ear diseases is questionable in adult rhinoceroses, except maybe in case of severe lesions. However, very good quality images were obtained in neonates and it is reasonable to assume that lesions could be detected in older juveniles.

We noticed the fact that increasing obliquity decreased the contrast of our radiographs. This is a logical finding and related to the fixed vertical position of the grid in our study. The latter restricts the number of X-rays hitting the cassette when the angle relative to the grid moves away from 90°. Further studies would be needed to assess image quality if the grid stays perpendicular to the X-ray beam.

In human medicine, plain radiographs of the temporal bone have been completely replaced by CT to overcome the limitations of radiography (Nayak 2001). Unfortunately this modality is not accessible for the vast majority of clinicians dealing with rhinoceroses and is limited to the smaller and younger animals.

Even though not directly associated with the ear, radiography allowed us to assess the changes occurring with age in the caudal part of the skull of the southern white rhinoceros. Whereas the fronto-parietal junction is convex in the neonate, it becomes concave in the adult rhinoceros. The caudal part of the occipital bone is caudo-ventrally oriented in neonates but becomes rostro-ventrally oriented in the adult. The external occipital protuberance also becomes much more prominent with age. Associated with this last finding is the extreme pneumatisation of the temporal and occipital bones with a sinus that looks continuous rostrally with the frontal sinus. Furthermore, suture lines similar to those observed in foals were observed (Butler et al. 2017). It is unfortunate that case 2, aged 4 months old, was not radiographed to get a better understanding of the changes happening with age at the caudal aspect of the skull.

5.3 Computed tomographic anatomy of the ear

Similar to what has been described in horses and people, CT appeared as a very valuable imaging modality when investigating the caudal skull of the southern white rhinoceros (Joshi et al. 2012; Manso-Díaz et al. 2015; Morrow et al. 2000; Nayak 2001). Even though not readily accessible in the majority of clinical cases, it could help to overcome the limitations of radiographs observed in the present study when evaluating this complex region where numerous osseous and soft tissue structures are superimposed. In particular, the external ear canal, tympanic bulla and petrous part of the temporal bone with its contained structures are clearly visible. The size of the animal did influence the image quality, as previously noticed (Fritsch et al. 2004). This is not surprising because larger animals are obviously wider, have a thicker skin and required thicker slice thickness (3mm in our larger cases) leading to images with a lower resolution. Whereas slice thicknesses from 2 to 10mm have been reported when investigating the temporal bone in horses, in human paediatric medicine, where high resolution is needed to investigate congenital hearing loss, slice thickness as little as 0.3mm is used (Joshi et al. 2012; Pownder et al. 2010). It is expected that newer generation CT scanners than the dual-slice we used in most of our study would improve image quality even in bigger animals.

Studies describing the CT anatomy of the equine head were used to identify the visible structures in our southern white rhinoceroses (Morrow et al. 2000; Smallwood et al. 2002). However the region of the temporal bone has a complex anatomy and some structures might have been missed. Age-related differences in the CT anatomy of the skull of the rhinoceros were observed, such as the presence of fibrous suture lines between individual bones. This is also similar to what has been reported between foals and adult horses (Smallwood et al. 2002). Nevertheless, one must remember that when looking at equine CTs, various temporal bone fissure lines (*fissura petrotympanica, fissura petrosquamosa, fissura tympanomastoidea, fissura tympanosquamosa*) can show diverse degree of fusion, which are not age related (Pownder et al. 2010). It is currently unknown if the same hold true for the southern white rhinoceros. This warrants further investigation.

5.4 Micro-anatomy of the ear

Micro-CT imaging allowed us to acquire excellent images of the tympanic membrane, middle ear and inner ear structures on all our samples. We were able to describe the relevant micro-anatomy of these structures in the southern white rhinoceros and to create virtual models of the auditory ossicles and bony labyrinth.

The mean image resolution in the present study was 39.5µm per voxel. This is similar to previous reports modeling the human middle ear where voxel sizes ranging from 19.5 to 76.0µm were used (Lee et al. 2010; Wang et al. 2007). However, the most recent studies investigating the human inner ear now use much higher resolutions, between 5.5 and 15µm per voxel (Glueckert et al. 2018; van den Boogert et al. 2018). One of the main limitations of using such high-resolutions is the comparatively long exposure and hence scanning time per specimen. The scanning time with our parameters was just above an hour. The only previous study using micro-CT on the ear in the rhinoceros had a higher voxel size of 126-309µm and did not describe the actual anatomy of the region (Schellhorn 2018).

The parameters used were 100kV and 100µA. This is comparable to previous reports where values between 40-70kV and 114-200µA were used in human samples (Glueckert et al. 2018; Wiet et al. 2005). The higher kV can be explained by the superior size of our rhinoceros samples.

The temporal bone specimens we scanned were fixed in formalin. This technique has been previously used in human studies (Wiet et al. 2005). It prevents movement that could occur with frozen samples melting during image acquisition. However identification of soft tissue structures was sometimes difficult. Alternative techniques to formalin-fixed micro-CT imaging are possible in order to better describe the soft tissue structures of the middle and inner ear of the southern white rhinoceros. For example, 3D virtual models of the human ear were previously obtained from scanned histological sections, allowing visualization of muscles, nerves and vessels (Green et al. 1990; Sorensen et al. 2002; Wang et al. 2007). Yet this technique can display compression artifacts and imperfect alignment. Another option would be to add high-field MRI images to our micro-CT images to include soft tissue structures in our model (Wiet et al. 2005; Wiet et al. 2002). Finally, recent reports showed the benefits of fixing temporal bones with osmium tetroxide as a contrast enhancer and decalcifying them with EDTA. This process gives extreme detail of the membranous labyrinth and neural structures of the human inner ear, permitting observation of individual neurons and of the organ of Corti (Glueckert et al. 2018; van den Boogert et al. 2018).

The auditory ossicles were visible on all samples and 3D models we generated. Whereas the *stapes* and *incus* had a shape similar to their human or equine counterparts, the *malleus* showed a unique appearance with a long rostral branch projecting latero-distally to the *manubrium*. This is probably what Owen (1866) described as a bifid head of the *malleus*. This rostral branch could represent an overdeveloped form of the muscular process observed in ruminants, where the tensor tympani muscle normally inserts (Botti et al. 2006). Alternatively, this rostral branch is more likely to be the *processus gracilis* and associated bony lamella, as described by Doran (1876). Further details about this rostral branch and its potential function could be obtained using micro-dissection. In addition, no particular muscle process, as observed in cattle, was observed on the *stapes* for the stapedius muscle.

It has previously been stated that the most obvious variation in the inner ear of mammals comes with the number of turns of the cochlear coil (Webster 1966). Whereas 2.5 to 2.75 turns have been described in the human cochlea (Curtin et al. 2011; Green et al. 1990) and 3 turns in the equine one (Collin 2006), only two turns were visible on our images of the southern white rhinoceros.

Distinguishing the perilymphatic spaces from the endolyphatic space and visualization of the small structures of the membranous labyrinth was not possible on our images. This could be investigated in future studies using special fixatives or higher scanning resolutions (van den Boogert et al. 2018).

The orientation of the semi-circular canals in the southern white rhinoceros seems similar to what has been described in men and horses (Collin 2006; Green et al. 1990).

Looking at the volume of the inner ear, it is interesting to note that despite their important size, southern white rhinoceroses have values very similar to humans. Indeed, we report a volume of 224.41mm^3 which is comparable to 192.5-227.8mm^3 reported in people (Buckingham & Valvassori 2001; Melhem et al. 1998). This could partially be explained by the shorter cochlea in the rhinoceros. However none of those studies used high resolution micro-CT images, which makes an accurate comparison difficult to perform.

The paths of the nerves (mainly facial) and vessels (internal carotid artery and jugular bulb) were somewhat detectable using human descriptions, but yet appeared difficult with some variations from what has been described in men (Moon & Lee 2014; Nayak 2001; Qiu et al. 2003). Once again, additional imaging modalities, micro-dissection and histological studies could help in better describing these paths.

It is anticipated that more 3D models could be extracted from our micro-CT images. However because extraction and segmentation processes are time consuming, we focused on the auditory ossicles and osseous labyrinth. Previous reports mention 2 to 3 person-months to create a full 3D virtual model of the human temporal bone (Wang et al. 2006). Luckily, newer image processing algorithms could expedite this step (van den Boogert et al. 2018).

This study describes the anatomy of the middle and inner ear of the southern white rhino using micro-CT imaging. Despite some unique particularities, it shows many similar traits to its well described human and equine counterparts. Further investigations are needed in order to provide a complete virtual model including both soft and bone tissues of this difficultly accessible region.

CONCLUSION

We were able to describe many features of the gross, radiographic, computed tomographic and micro-CT anatomy of the ear of the southern white rhinoceros. Comparing our results with data from the equine and human fields we were able to identify structures and show some traits that are particular to the rhinoceros.

Limitations of our study lie in the low number of cases and the fact that not all the heads could undergo all the imaging modalities and dissection. Additionally, post-mortem artifacts such as air in the soft tissues and fluid in the hollow cavities of the head sometimes made interpretation of the images sometimes difficult.

However, we think this study will provide anatomists, wildlife veterinarians and imagers with some basics that could be used as a reference to better understand the complex anatomical features of the ear region of the southern white rhinoceros.

Further research is still possible and needed. For example, MRI images acquired from some of our samples could be used and combined with anatomic slices, CT and micro-CT images to create an atlas of the southern white rhinoceros ear region. Similarly, obtaining more measurements from animals of different ages could be used to draw “growth curves” of the size of the head, pinna, tympanic bulla, petrous part of the temporal bone and also illustrate in details all the changes occurring with age in the head of the southern white rhinoceros.

APPENDICES

Appendix A: Owner consent form

Owner detail	
Surname :	Name :
Email address	
Rhino detail	
Name :	
Microchip nr :	
Sex : M / F	DOB :
Estimated weight :	
I ______________________________ hereby give consent for the above mentioned rhino to be evaluated and radiographed as part of the study entitled "Gross morphology, radiology and computed tomography of the ear of the southern white rhinoceros (*Ceratotherium simum simum*)" conducted by Dr. Mickaël Robert, Prof. Ann Carstens and Prof. Gerhard Steenkamp. I am responsible for and able to give consent for the above mentioned rhino. I am aware that : - no individual radiographic report will be issued by the authors, but that I may have access to the results of this study - no compensation will be payable to the animal's owner or anybody else and that all research associated costs will be covered by the researcher(s). - this form would serve to fully indemnify the University of Pretoria and the pre-cited researchers against any future claims resulting from the specified procedure by or on behalf of the animal's owner. - no material of any kind, including data and research findings, obtained or resulting from the procedure, would be passed on to any third party or used for any purpose other than that specified in this form, except with the written consent of the undersigned owner of the animal. - no personal information will be disclosed but may be used unanimous in publications. As owner it is my right to withdraw my animal/s from the trial	
Signature	Date

UNIVERSITEIT VAN PRETORIA
UNIVERSITY OF PRETORIA
YUNIBESITHI YA PRETORIA

Appendix B: Ethics approval from the Animal Ethics Committee of the University of Pretoria

UNIVERSITEIT VAN PRETORIA
UNIVERSITY OF PRETORIA
YUNIBESITHI YA PRETORIA

Animal Ethics Committee

PROJECT TITLE	**Gross morphology, radiology and computed tomography of the ear region of the Southern White Rhinoceros (*Ceratotherium simum simum*)**
PROJECT NUMBER	**V088-18**
RESEARCHER/PRINCIPAL INVESTIGATOR	**Dr. M Robert**

STUDENT NUMBER (where applicable)	**U_04944764**
DISSERTATION/THESIS SUBMITTED FOR	**MSc**

ANIMAL SPECIES/SAMPLE	**Southern White Rhinoceros (*Ceratotherium simum simum*)**	
NUMBER OF SAMPLES	**4-8 heads (Previously approved V063-15 and V023-12)**	
Approval period to use animals for research/testing purposes		**October 2018 – October 2019**
SUPERVISOR	**Prof. G Steenkamp**	

KINDLY NOTE:

Should there be a change in the species or number of animal/s required, or the experimental procedure/s - please submit an amendment form to the UP Animal Ethics Committee for approval before commencing with the experiment

APPROVED	Date	30 October 2018
CHAIRMAN: UP Animal Ethics Committee	Signature	

S4285-15

Appendix C: Permission to do research in terms of section 20 of the animal diseases act (ACT NO.35 of 1984).

agriculture, forestry & fisheries

Department:
Agriculture, Forestry and Fisheries
REPUBLIC OF SOUTH AFRICA

Directorate Animal Health, Department of Agriculture, Forestry and Fisheries
Private Bag X138, Pretoria 0001

Enquiries: Mr Herry Gololo • Tel: +27 12 319 7532 • Fax: +27 12 319 7470 • E-mail: HerryG@daff.gov.za
Reference: 12/11/1/1/8

Dr Mickaël Robert
Department of Companion Animal Clinical Studies
Faculty of Veterinary Science
Old Soutpan Road
Onderstepoort, 0110

Email: mickael.robert@up.ac.za; CC: Mario.smuts@up.ac.za

Dear Dr Robert,

RE: PERMISSION TO DO RESEARCH IN TERMS OF SECTION 20 OF THE ANIMAL DISEASES ACT, 1984 (ACT NO. 35 of 1984)

Your application, submitted on 29 March 2019, requesting permission under Section 20 of the Animal Disease Act, 1984 (Act No. 35 of 1984) to perform a research project or study, refers.

I am pleased to inform you that permission is hereby granted to perform the following research/study, "*Gross morphology, radiology and computed tomography of the ear of the Southern White rhinoceros (Cerathotherium simum simum)*" with the following conditions:

Conditions:

1. This study is approved as per the application form dated 18 March 2019 and the correspondence thereafter. Written permission from the Director: Animal Health must be obtained prior to any deviation from the conditions approved for this study under this Section 20 permit. Please apply in writing to HerryG@daff.gov.za
2. If required, an application for an extension must be made by the responsible researcher at least one month prior to the expiry of this Section 20 approval.

- 1 -

3. This permission does not relieve the researcher of any responsibility which may be placed on him by any other act of the Republic of South Africa;
4. All potentially infectious material utilised or collected during the study is to be destroyed at the completion of the study. Records must be kept for five years for audit purposes. A dispensation application may be made to the Director Animal Health in the event that any of the above is to be stored or distributed;
5. Samples to be transported must be packaged in compliance with the Regulations of the National Road Traffic Act, 1996 (Act No 93 of 1996) or IATA requirements;
6. Heads may be harvested from deceased rhinoceroses at Buffalo Dream Ranch;
7. The collected rhinoceros heads may be temporarily stored at -20 degree Celcius in a dedicated freezer in the Department of Companion Animal Clinical Studies;
8. The Waste group must be used for the disposal of the rhinoceros heads;
9. This section 20 expires on 31 August 2019.

Title of research/study: "Gross morphology, radiology and computed tomography of the ear of the Southern White rhinoceros (*Cerathotherium simum simum*)."
Researcher (s): Dr Dr Mickaël Robert
Institution: Department of Companion Animal Clinical Studies
Faculty of Veterinary Science, Onderstepoort
Your Ref./ Project Number: 12/11/1/1/8
Our ref Number:

Kind regards,

Maja.

DR. MPHO MAJA
DIRECTOR OF ANIMAL HEALTH
Date: 2019 -04- 15

REFERENCES

Anonymous. 2012. *Vietnam driving increase in rhino poaching: experts* [Online]. Available: http://www.thanhniennews.com/society/vietnam-driving-increase-in-rhino-poaching-experts-6952.html [Accessed 01/08/2018].

Anonymous. 2018a. *Buyers of Rhino Horn* [Online]. Available: http://www.poachingfacts.com/faces-of-the-poachers/buyers-of-rhino-horn/ [Accessed 01/08/2018].

Anonymous. 2018b. *Rhino poaching statistics* [Online]. Available: http://www.poachingfacts.com/poaching-statistics/rhino-poaching-statistics/ [Accessed 01/08/2018].

Baptiste, K. E., Naylor, J. M., Bailey, J., Barber, E. M., Post, K. & Thornhill, J., 2000, 'A function for guttural pouches in the horse', *Nature* 403**,** 382-3.

Barone, R. 2010a. *Anatomie comparée des mammifères domestiques. Tome 1: Ostéologie,* 5th Ed. Paris, Vigot.

Barone, R. 2010b. *Anatomie comparée des mammifères domestiques. Tome 2: Arthrologie et Myologie,* 5th Ed. Paris, Vigot.

Barone, R. 2010c. *Anatomie comparée des mammifères domestiques. Tome 7: Neurologie II,* Paris, Vigot.

Barone, R. 2011. *Anatomie comparée des mammifères domestiques. Tome 5: Angiologie,* 2nd Ed. Paris, Vigot.

Botti, M., Secci, F., Ragionieri, L., Dessole, A. A. & Acone, F., 2006, 'Auditory ossicles in the ruminants: Comparative morphological analysis with the analogues formations of horse', *Annali della Facoltà di Medicina Veterinaria-Università di Parma (Italy)*.

Buckingham, R. A. & Valvassori, G. E., 2001, 'Inner ear fluid volumes and the resolving power of magnetic resonance imaging: can it differentiate endolymphatic structures?', *Ann Otol Rhinol Laryngol* 110**,** 113-7.

Buss, P. E., 2018. Personal communication.

Butler, J. A., Colles, C. M., Dyson, S. J., Kold, S. E. & Poulos, P. W. 2017. *Clinical radiology of the horse*, John Wiley & Sons.

Cave, A. J. E., 1974, 'The epipharyngeal bursa in the Rhinocerotidae', *Journal of Zoology* 172**,** 133-145.

CITES. 2017. *Appendices I, II and III* [Online]. Available: https://www.cites.org/eng/app/appendices.php [Accessed 24/09/2018].

Collin, B. 2006. *Anatomie du cheval,* Liège, Derouaux Ordina Editions.

Curtin, H., Gupta, R. & Bergeron, R., 2011, 'Embryology, anatomy and imaging of the temporal bone', *Head and Neck Imaging. 5th ed. Philadelphia: Elsevier Mosby* 1058.

De Vos, V., 1978, 'Congenital unilateral aotus in a black rhinoceros diceros bicornis bicornis (Linn., 1758)', *J S Afr Vet Assoc* 49**,** 71.

Dinerstein, E., 2011, 'Family Rhinocerotidae (rhinoceroses)', in D. E. Wilson & R. A. Mittermeier (eds.), *Handbook of the mammals of the world. Vol. 2. Hoofed mammals*, pp. 144-181, Lynx Edicions, Barcelona.

Divers, T. J., Ducharme, N. G., De Lahunta, A., Irby, N. L. & Scrivani, P. V., 2006, 'Temporohyoid Osteoarthropathy', *Clinical Techniques in Equine Practice* 5**,** 17-23.

Doran, A. H. G., 1876, 'On the comparative anatomy of the auditory ossicles of the Mammalia', *Proceedings of the Royal Society of London* 25**,** 101-109.

Dudley, R. J., Wood, S. P., Hutchinson, J. R. & Weller, R., 2015, 'Radiographic Protocol and Normal Anatomy of the Hind Feet in the White Rhinoceros (Ceratotherium Simum)', *Veterinary Radiology & Ultrasound* 56**,** 124-132.

Emslie, R. 2012. *Ceratotherium simum. The IUCN Red List of Threatened Species 2012: e.T4185A16980466.* [Online]. Available: http://dx.doi.org/10.2305/IUCN.UK.2012.RLTS.T4185A16980466.en [Accessed 08/05/2018].

Emslie, R. H., Milliken, T., Talukdar, B., Ellis, S., Adcock, K. & Knight, M. H. 2016. African and Asian rhinoceroses–status, conservation and trade: a report from the IUCN

Species Survival Commission (Iucn Ssc) African and Asian Rhino Specialist Groups and Traffic to the Cites Secretariat Pursuant to Resolution Conf. 9.14 (Rev. Cop15). Convention on International Trade in Endangered Species of Wild Fauna and Flora (CITES) Secretariat, Geneva.

Endo, H., Manglai, Fujisawa, M., Kurohmaru, M. & Hayashi, Y., 1998, 'The guttural pouch is not present in the white rhinoceros (Ceratotherium simum); morphology of the eustachian tube and nasopharynx', *Anat Histol Embryol* 27**,** 327-30.

Endo, H., Taru, H., Hayashida, A., Kimura, J., Itou, T., Koie, H. & Sakai, T., 2009, 'Absence of the Guttural Pouch in a Newborn Indian Rhinoceros Demonstrated by Three-Dimensional Image Observations', *Mammal Study* 34**,** 7-11.

Freeman, D. E. & Hardy, J., 2012, 'Guttural Pouch', in J. A. Auer & J. A. Stick (eds.), *Equine Surgery*, 4th Ed, pp. 623-642, W.B. Saunders, Saint Louis.

Fritsch, G., Frey, R., Hermes, R., Goeritz, F., Strauss, G., Wibbett, G. & Hildebrandt, T. B. 2004. Comparative study on rhinoceros head anatomy using endoscopy, computed tomography (CT) and gross anatomy. Proceedings of the AAZV, AAWV, WDA Joint Conference. 128-129.

Galateanu, G., Hildebrandt, T. B., Maillot, A., Etienne, P., Potier, R., Mulot, B., Saragusty, J. & Hermes, R., 2013, 'One Small Step for Rhinos, One Giant Leap for Wildlife Management- Imaging Diagnosis of Bone Pathology in Distal Limb', *PLoS ONE* 8**,** e68493.

Galateanu, G., Hermes, R., Saragusty, J., Göritz, F., Potier, R., Mulot, B., Maillot, A., Etienne, P., Bernardino, R., Fernandes, T., Mews, J. & Hildebrandt, T. B., 2014, 'Rhinoceros Feet Step Out of a Rule-of-Thumb: A Wildlife Imaging Pioneering Approach of Synchronized Computed Tomography-Digital Radiography', *PLoS ONE* 9**,** e100415.

Gerard, M. P., Glyphis, Z. G., Crawford, C., Blikslager, A. T. & Marais, J., 2018, 'Identification of a Nasoconchal Paranasal Sinus in the White Rhinoceros (Ceratotherium Simum)', *J Zoo Wildl Med* 49**,** 444-449.

Glueckert, R., Johnson Chacko, L., Schmidbauer, D., Potrusil, T., Pechriggl, E. J., Hoermann, R., Brenner, E., Reka, A., Schrott-Fischer, A. & Handschuh, S., 2018, 'Visualization of the Membranous Labyrinth and Nerve Fiber Pathways in Human and Animal Inner Ears Using MicroCT Imaging', *Frontiers in Neuroscience* 12.

Goddard, J., 1969, 'A note on the absence of pinnae in the black rhinoceros', *East African Wildlife Journal* 7**,** 178-180.

Green, J. D., Jr., Marion, M. S., Erickson, B. J., Robb, R. A. & Hinojosa, R., 1990, 'Three-dimensional reconstruction of the temporal bone', *Laryngoscope* 100**,** 1-4.

Hahn, C., 2015, 'Chapter 83 - Diseases Associated With Clinical Signs Originating From Cranial Nerves A2 - Sprayberry, Kim A', in N. E. Robinson (ed.) *Robinson's Current Therapy in Equine Medicine (Seventh Edition)*, pp. 361-365, W.B. Saunders, St. Louis.

Hinchcliffe, R. & Pye, A., 2009, 'Variations in the middle ear of the Mammalia', *Journal of Zoology* 157**,** 277-288.

Hyrtl, J. 1873. *Die Corrosions-Anatomie und ihre Ergebnisse,* Vienna, Braumüller.

ICVGAN. 2017. *Nomina Anatomica Veterinaria,* 6th Ed. W. a. O. V. A. (W.A.V.A.). Available: http://www.wava-amav.org/downloads/nav_6_2017.zip [Accessed 11/12/2019].

Joshi, V. M., Navlekar, S. K., Kishore, G. R., Reddy, K. J. & Kumar, E. C. V., 2012, 'CT and MR Imaging of the Inner Ear and Brain in Children with Congenital Sensorineural Hearing Loss', *RadioGraphics* 32**,** 683-698.

Khairuddin, N. H., Sullivan, M. & Pollock, P. J., 2015, 'Angiographic Variation of the Internal Carotid Artery and its Branches in Horses', *Vet Surg* 44**,** 784-9.

Knight, M., 2017, 'African Rhino Specialist Group report', *Pachyderm* 58**,** 17-35.

Lee, D. H., Chan, S., Salisbury, C., Kim, N., Salisbury, K., Puria, S. & Blevins, N. H., 2010, 'Reconstruction and exploration of virtual middle-ear models derived from micro-CT datasets', *Hearing Research* 263**,** 198-203.

Lemonde.Fr. 2018. Available: http://www.lemonde.fr/planete/article/2018/03/20/kenya-mort-de-sudan-le-dernier-rhinoceros-male-blanc-du-nord_5273465_3244.html [Accessed 8th May 2018].

Lepage, O. M., 2007, 'Disorders of the Guttural Pouches', in P. Lekeux (ed.) *Equine Respiratory Diseases*, pp. International Veterinary Information Service (www.ivis.org), Ithaca, NY

Manso-Díaz, G., García-López, J. M., Maranda, L. & Taeymans, O., 2015, 'The role of head computed tomography in equine practice', *Equine Veterinary Education* 27**,** 136-145.

Melhem, E. R., Shakir, H., Bakthavachalam, S., Macdonald, C. B., Gira, J., Caruthers, S. D. & Jara, H., 1998, 'Inner ear volumetric measurements using high-resolution 3D T2-weighted fast spin-echo MR imaging: initial experience in healthy subjects', *AJNR Am J Neuroradiol* 19**,** 1819-22.

Miller, M. A. & Buss, P. E., 2014, 'Rhinoceridae (Rhinoceroses)', in R. E. Miller & M. Fowler (eds.), *Fowler's Zoo and Wild Animal Medicine, Volume 8*, pp. 538-547, Elsevier, Saint Louis.

Milliken, T., Emslie, R. H. & Talukdar, B. 2009. African and Asian rhinoceroses–status, conservation and trade: a report from the IUCN Species Survival Commission (IUCN/SSC) African and Asian Rhino Specialist Groups and TRAFFIC to the CITES Secretariat pursuant to Resolution Conf 9.14 (Rev. CoP14) and Decision 14.89. Convention on International Trade in Endangered Species of Wild Fauna and Flora (CITES) Secretariat, Geneva.

Milliken, T., Shaw, J. & Emslie, R. H. 2012. *The South Africa–Vietnam rhino horn trade nexus: A deadly combination of institutional lapses, corrupt wildlife industry professionals and Asian crime syndicates,* Traffic. Johannesburg.

Moon, I. S. & Lee, W.-S., 2014, 'Internal Carotid Artery in the Middle Ear', *New England Journal of Medicine* 371.

Morrow, K. L., Park, R. D., Spurgeon, T. L., Stashak, T. S. & Arceneaux, B., 2000, 'Computed tomographic imaging of the equine head', *Vet Radiol Ultrasound* 41**,** 491-7.

Nayak, S., 2001, 'Segmental anatomy of the temporal bone', *Seminars in Ultrasound, CT and MRI* 22**,** 184-218.

Ngene, S., Bitok, E., Mukeka, J., Gakuya, F., Omondi, P., Kimetei, K., Watol, Y., Kariuki, L. & Ouma Okita, B., 2011, 'Census and ear-notching of black rhinoceros (Diceros bicornis michaeli) in Tsavo East National Park, Kenya', *Pachyderm* 49**,** 61-69.

Owen-Smith, R. N., 2013, 'Ceratotherium simum - white rhinoceros (grass rhinoceros, square-lipped rhinoceros)', in J. Kingdon & M. Hoffmann (eds.), *Mammals of Africa - Volume V*, pp. 446-454, Bloomsbury, London.

Owen, R. 1866. *On the anatomy of vertebrates - Volume III: Mammals,* London., Longmans, Green and Co.

Patton, F., 2017, 'The use of ear tufts to assist in the identification of individual black rhinos', *Pachyderm* 58**,** 148-151.

Pollock, P. J., 2007, 'Diagnosis and management of guttural pouch mycosis', *Equine Veterinary Education* 19**,** 522-527.

Portas, T. J., Hermes, R., Bryant, B. R., Göritz, F., Thorne, A. R. & Hildebrandt, T. B., 2006, 'Anesthesia and Use of a Sling System to Facilitate Transvaginal Laparoscopy in a Black Rhinoceros (Diceros Bicornis Minor)', *Journal of Zoo and Wildlife Medicine* 37**,** 202-205.

Pownder, S., Scrivani, P. V., Bezuidenhout, A., Divers, T. J. & Ducharme, N. G., 2010, 'Computed Tomography of Temporal Bone Fractures and Temporal Region Anatomy in Horses', *Journal of Veterinary Internal Medicine* 24**,** 398-406.

Qiu, M. G., Zhang, S. X., Liu, Z. J., Tan, L. W., Wang, Y. S., Deng, J. H. & Tang, Z. S., 2003, 'Plastination and computerized 3D reconstruction of the temporal bone', *Clin Anat* 16**,** 300-3.

Quse, V. & Fernandes-Santos, R. C. 2014. *Tapir Veterinary Manual,* 2nd Ed. IUCN/SSC Tapir Specialist Group (TSG).

Robin Des Bois, 2018, 'Notes on rhinoceros poaching', *On the Trail (Information and analysis bulletin on animal poaching and smuggling)* 19**,** 83-91.
Rooney, J. R., 1996, 'Respiratory system. ', in J. R. Rooney & J. L. Robertson (eds.), *Equine Pathology*, pp. 33-35, State University Press, Ames: Iowa
Saban, R., 1970, 'La musculature peauciere de la tete et du cou chez Rhinoceros unicornis Linne, 1758', *Gegenbaurs Morphologisches Jahrbuch* 115**,** 418-443.
Schellhorn, R., 2018, 'A potential link between lateral semicircular canal orientation, head posture, and dietary habits in extant rhinos (Perissodactyla, Rhinocerotidae)', *J Morphol* 279**,** 50-61.
Slovis, N., 2012, 'Equine otitis media-interna', *Equine Veterinary Education* 24**,** 276-278.
Smallwood, J. E., Wood, B. C., Taylor, W. E. & Tate, L. P., Jr., 2002, 'Anatomic reference for computed tomography of the head of the foal', *Vet Radiol Ultrasound* 43**,** 99-117.
Sorensen, M. S., Dobrzeniecki, A. B., Larsen, P., Frisch, T., Sporring, J. & Darvann, T. A., 2002, 'The visible ear: a digital image library of the temporal bone', *ORL J Otorhinolaryngol Relat Spec* 64**,** 378-81.
Steenkamp, G., 2017. Personal communication.
Steenkamp, G., 2018. Personal communication.
TRAFFIC. 2018. *South Africa: rhino poaching in 2017 almost matches 2016 figure, with KwaZulu Natal now bearing the brunt* [Online]. Cambridge. Available: https://www.traffic.org/news/south-africa-rhino-poaching-in-2017-almost-matches-2016-figure-with-kwazulu-natal-now-bearing-the-brunt/ [Accessed 11/12/2019].
Valverde, A., Crawshaw, G. J., Cribb, N., Bellei, M., Gianotti, G., Arroyo, L., Koenig, J., Kummrow, M. & Costa, M. C., 2010, 'Anesthetic management of a white rhinoceros (Ceratotherium simum) undergoing an emergency exploratory celiotomy for colic', *Veterinary Anaesthesia and Analgesia* 37**,** 280-285.
Van Den Boogert, T., Van Hoof, M., Handschuh, S., Glueckert, R., Guinand, N., Guyot, J.-P., Kingma, H., Perez-Fornos, A., Seppen, B., Johnson Chacko, L., Schrott-Fischer, A. & Van De Berg, R., 2018, 'Optimization of 3D-Visualization of Micro-Anatomical Structures of the Human Inner Ear in Osmium Tetroxide Contrast Enhanced Micro-CT Scans', *Frontiers in Neuroanatomy* 12.
Vicq-D'azyr, F. & Cloquet, H. 1819. *Encyclopédie Méthodique, Tome 3: Système Anatomique; Mammifères Et Oiseaux,* Paris, Veuve Agasse.
Walker, A. M., Sellon, D. C., Cornelisse, C. J., Hines, M. T., Ragle, C. A., Cohen, N. & Schott, H. C., 2nd, 2002, 'Temporohyoid osteoarthropathy in 33 horses (1993-2000)', *J Vet Intern Med* 16**,** 697-703.
Walzer, C., Göritz, F., Hermes, R., Nathan, S., Kretzschmar, P. & Hildebrandt, T., 2010, 'Immobilization and Intravenous Anesthesia in a Sumatran Rhinoceros (Dicerorhinus sumatrensis)', *Journal of Zoo and Wildlife Medicine* 41**,** 115-120.
Wang, H., Merchant, S. N. & Sorensen, M. S., 2007, 'A downloadable three-dimensional virtual model of the visible ear', *ORL J Otorhinolaryngol Relat Spec* 69**,** 63-7.
Wang, H., Northrop, C., Burgess, B., Liberman, M. C. & Merchant, S. N., 2006, 'Three-dimensional virtual model of the human temporal bone: a stand-alone, downloadable teaching tool', *Otol Neurotol* 27**,** 452-7.
Webster, D. B., 1966, 'Ear Structure and Function in Modern Mammals', *American Zoologist* 6**,** 451-466.
Wiet, G. J., Schmalbrock, P., Powell, K. & Stredney, D., 2005, 'Use of ultra-high-resolution data for temporal bone dissection simulation', *Otolaryngol Head Neck Surg* 133**,** 911-5.
Wiet, G. J., Stredney, D., Sessanna, D., Bryan, J. A., Welling, D. B. & Schmalbrock, P., 2002, 'Virtual temporal bone dissection: an interactive surgical simulator', *Otolaryngol Head Neck Surg* 127**,** 79-83.
Witmerlab. 2012. *The visible interactive rhino.* [Online]. Available: https://people.ohio.edu/witmerl/3D_rhino.htm [Accessed 24/09/2018].

Zeiler, G. E. & Stegmann, G. F., 2012, 'Anaesthetic management of a 10-month-old white rhinoceros (Ceratotherium simum) calf for emergency exploratory celiotomy', *Journal of the South African Veterinary Association* 83.